39(4)

USC DISCARD

RECEIVED
SEP 44 1989

気象庁欧文海洋報告

第39巻 第1–2号

THE OCEANOGRAPHICAL MAGAZINE

Vol. 39 Nos. 1-2

CONTENTS

KADOWO, K. and T. SAGI : Distribution of nitrogen compounds and chlorophyll-a concentrations in the euphotic zone 1

OHYAMA, J., F. MARUYAMA and Y. DOKIYA : Distribution and behavior of bismuth in Tokyo Bay 11

KOHSHI, T : Numerical forecast of storm surges on real time basis 21

KANO, Y., K. SATO and S. SHIRATO : Statistical study on sea ice in the Okhotsk Sea observed by GMS for 10 years 43

Library
NOAA, National Marine Fisheries Service
SWFC Honolulu Laboratory F/SWC2
2570 Dole Street
Honolulu, HI 96822-2396

Published by the Japan Meteorological Agency

March, 1989

投稿規定

1　資　格

原則として，気象庁職員に限る。ただし，気象庁職員との連名の場合は，この限りでない。

2　論文及び報文（以下「論文等」という）の内容

未発表の原稿で，海洋（物理・化学・生物・地質など）及び海上気象（波浪・海氷・海気相互関係など）に関する論文並びに気象庁における海洋・海上気象業務の活動，そのために開発された測器及び方法に関する報文など。

3　書き方

(1) 用語は，欧文（原則として英文）とする。

(2) 論文等には，英文（300語以内）及び和文（800字以内）の要約を付ける。要約は，方法・測器・実験・観測の結果・仮定・理論などの中味が読みとれるように留意し，なるべく指定の長さで簡潔に書く。

(3) 論文等の始めには，題名・著者名及所属機関名を明記する。和文の要約にも同様のことを明記する。

(4) 原稿は，厚手の用紙にダブルスペースでタイプする。

(5) 図は，白紙又は青方眼紙に墨入れし，図及び図中の文字の大きさは，印刷の際の縮小率を考えて作成する。特に重要な図は，投稿者が大きさを指定する。（印刷の都合上，希望どおりにならないこともある）

(6) 図（写真を含む）及び表には，必ず説明を付ける。図の説明文は，別紙にタイプする。折り込みの図及び表は，なるべく避ける。図及び表のそう入箇所を本文の欄外に記入する。

(7) 数式は，2行取りに書き，数式の文字及び記号をはっきりと説明する。

(8) 論文等の中に文献を引用する場合は，「ALLEN (1927)」又は「(ALLEN, 1927)」のように書く。

(9) 引用文献は，最後にまとめて付け，著者名のアルファベット順に並べる。書き方は次のようにする。

ALLEN, W.E. (1927): Surface catches of marine diatoms and dinoflagellates made by U.S.A. Pioneer in Alaskan waters in 1923. *Bull. Scripps Inst. Occanogr., Tech. Ser.* 1(4), 39–48.

BUDYKO, M. I. (1956): *The heat balance of the earth's surface.* Hydrometeorogical Publishing House, Leningrad, pp. 254.

VERONINS, G. and H. STOMMEL (1956): The action of a variable wind stress on a stratified ocean. *J. Mar. Res.*, 15(1), 43–75.

4　提出方法

投稿票を付け，本稿のほかにコピー（図及び表を含む）2部を添える。

5　送付先

気象庁海洋気象部海洋課

6　その他

論文等1編につき別刷り50部を著者に無料で送付する。

Oceanographical Magazine

編集委員長　Editor

荒　川　正　一，S. ARAKAWA*

編集委員　Editorial Board

宇　治　　豪，	T. UJI*	鷺　　猛，	T. SAGI*
遠　藤　昌　宏，	M. ENDOH**	杉　村　行　勇，	Y. SUGIMURA**
大　山　準　一，	J. OHYAMA*	羽　鳥　光　彦，	M. HATORI*
斎　藤　利　夫，	T. SAITO*	湊　　信　也，	S. MINATO***
佐　伯　理　郎，	M. SAIKI*	南　　秀　人，	H. MINAMI*

*気　象　庁　JAPAN METEOROLOGICAL AGENCY
**気象研究所　METEOROLOGICAL RESEARCH INSTITUTE
***気象大学校　METEOROLOGICAL COLLEGE

The Oceanographical Magazine
Vol. 39, Nos. 1-2, pp. 1 to 9, March 1989

Distributions of nitrogen compounds and chlorophyll-a concentrations in the euphotic zone

Koji KADONO and Takeshi SAGI
Japan Meteorological Agency

(Received November 17, 1988; Accepted November 31, 1988)

Abstract: To confirm the regional oceanographic features controlling biological production, the distribution of nitrogen compounds and chlorophyll-a concentrations in the euphotic zone are examined. The depth of euphotic zone estimated from the transparency reading by Secchi disk varies regionally from 100 m in the Subtropics to 27 m in the continental shelf in the East China Sea.

In those euphotic zones, ammonia rich water (1–2 μmol/l) are found in summer in the regions far from east of the Yangtze river, off the Kii channel and off the southern Hokkaido. The chlorophyll-a concentration as an index of plankton biomass is high in these regions. Though the nitrate concentration is remarkably high in winter in the Oyashio region off the southern Hokkaido, a low chlorophyll-a concentration is observed in this region. Both concentrations of the nitrogen compounds and the chlorophyll-a are low in the Subtropics. It seems to suggest that the biological productivitie is limited by the temperature in the Oyashio region but by the depletion of nitrogen compounds in the Subtropics.

1. Introduction

The depletion mechanism of the nutrients in sea water is the uptake by biomass in the euphotic zone and the generation mechanism of them is the oxidative decomposition of organic matter in the deep layer. Accordingly, the concentration of inorganic nitrogen compounds lowers in the euphotic zone and then becomes the essential factor controlling the primary production in the ocean. The lowering of the N/P ratio at the surface in most areas of the ocean is also an example of the depletion of nitrogen (SAGI, 1978).

Vertical distributions of ammonia, nitrite and nitrate in the upper layer are shown in Fig. 1. These profiles were obtained by TAKATANI (1987) on board R.V. Ryofu Maru. The sea water is pumped up continuously through a long polyethylene tube and analyzed automatically with a auto-analyzer. Two or three maxima of these nutrients concentrations appear in the upper layer. The maximum of Ammonia is ordinarily observed in the photosynthetic layer and that of nitrite generally appears near the compensation depth for photosynthesis, below which nitrate concentration increases rapidly with increasing depth.

However, there is little information in the upper layer about the mutual relations among various forms of concentrations of nitrogen compounds. To evaluate their mutual relation and to confirm the regional oceanographic features controlling biological production in the seas around Japan, seasonal changes and the mutual relations among ammonia, nitrite and nitrate concentrations in the euphotic zone are examined by using chlorophyll-a concen-

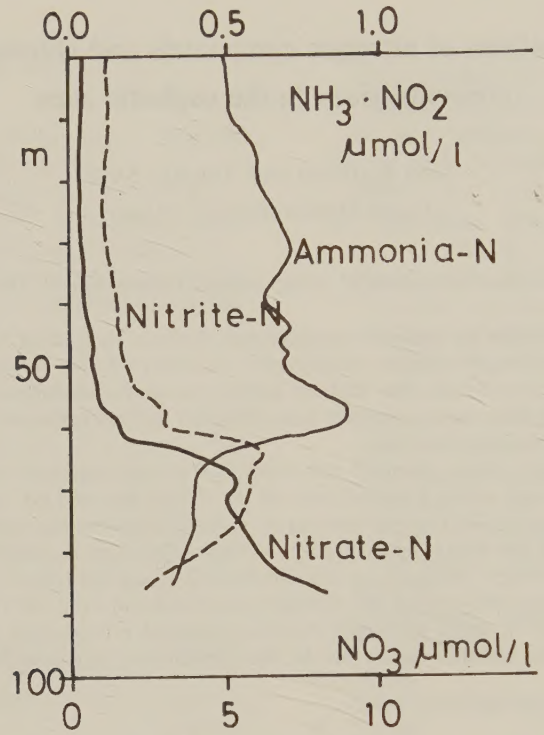

Fig. 1. Profiles of ammonia, nitrite and nitrate in the surface sea water at 35°15′N, 139°20′E.

tration as an index of plankton biomass in the present report.

2. Materials and methods

The names of research ships and dates of the observations which are related to this study are summarized in Table 1. The locations of the sampling stations are shown in Fig. 2 except for the long observation line at 155°E. Auto-analyzer systems for the determination of nutrients have been adopted routinely on these observations. Ammonia in sea water has been determined using indophenol method with nitroprusside. For the determination of nitrite in sea water two solutions of sulphanilamid hydrochloride and n-(1-naphthyl)ethylenediamine dihydrochloride have been used. Nitrate in sea water has been determined with copper cadmium reduction. And chlorophyll-a concentration has been measured by fluorometric technique.

The concentrations of nitrogen compounds in the upper layer vary vertically and locally controlling the biological production in the ocean. While, the biological production is also controlled by the light intensity and the temperature. The light intensity decreases with depth and varies with latitude and season. Accordingly, the mean concentrations of biochemical elements in the euphotic zone will be a great help in discussion the distribu-

Table 1 The names of the ships and the dates of the observations relevant to the present report.

Stations or observation line	Ship names	Dates	
		Winter	Summer
PH 1, 3, 6	Kofu Maru	1980～1985 (Feb.)	1980～1985 (Aug.)
PM 1, 5, 9	Seifu Maru	1980, 1984, 1985 (Feb.)	1980, 1984, 1985 (July)
PN 1, 4, 9	Chofu Maru	1980～1983 (Jan.)	1980～1983 (July)
PK 1, 9	Shumpu Maru	1980, 1982～1985 (Feb.)	1983, 1984 (July)
PT 1, 2, 5	Ryofu Maru	1980～1985 (Feb.)	1980～1984 (June)
at 155°E	Ryofu Maru	47°N～20°N 20°N～50°N	1969 (May) 1972 (June)

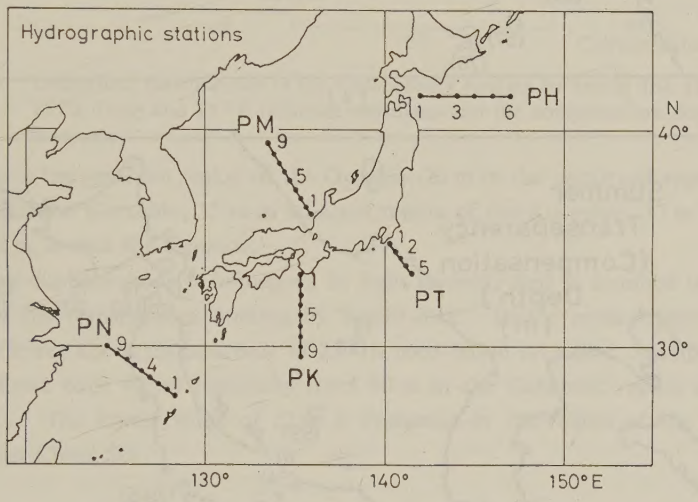

Fig. 2. Sampling stations and observation lines.

tion of nitrogen compounds in the upper layer. At the beginning the depth of euphotic zone is estimated from values of transparency reading by Secchi disk in each region.

3. Estimation of the depth of euphotic zone in each region

In order to estimate the depth of euphotic zone in each region, the transparency reading by Secchi disk are used in the data of several cruises. Those mean values in the seas around Japan are shown in Fig. 3 and in the western North Pacific along 155°E and 137°E meridians are shown in Fig. 4. Though values of transparency fluctuate as shown in Fig. 4, we can recognize the regional variation of transparency, i.e. 25 m in the northern region of the

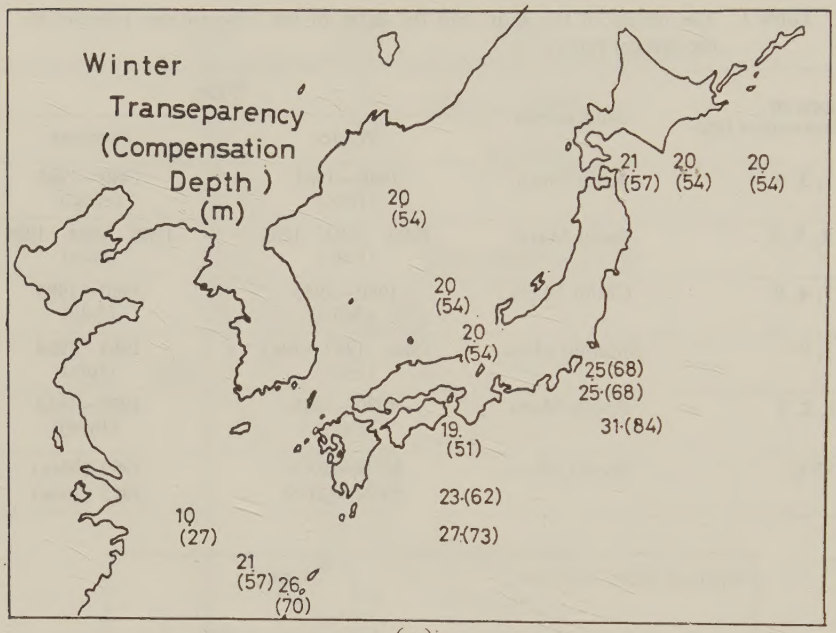

(a)

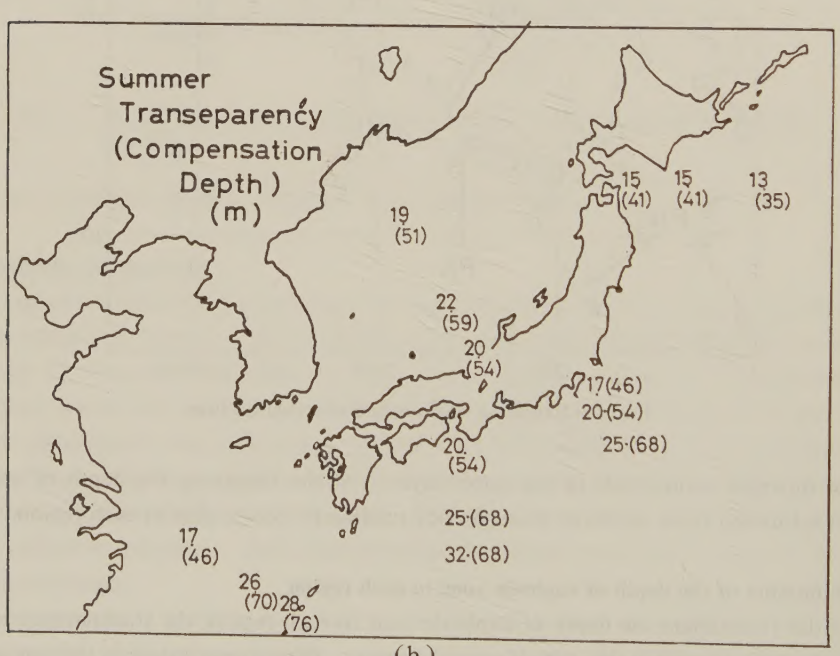

(b)

Fig. 3. Distributions of the transparency readings by Secchi disk and the compensation depths.

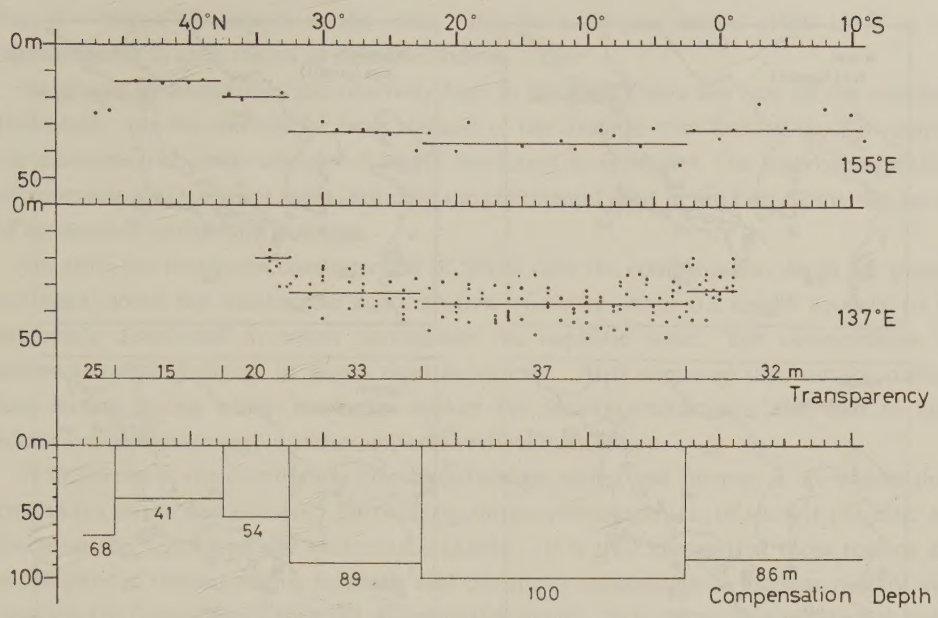

Fig. 4. Latitudinal distributions of the transparency reading by Secchi disk along 155°E (top) and 137°E (middle) meridians and the compensation depths (bottom).

Oyashio, 15 m in the southern region of the Oyashio, 20 m in the perturbed region between the Oyashio and the Kuroshio, 33 m in adjacent region of the Kuroshio, 37 m in the Subtropics and 32 m in near the Equator.

The depth of euphotic zone is influenced by light intensity and is assumed to be two or three times of the transparency reading by Secchi disk. In the present report the proportional coefficient about transparency of 2.7* is used based on a few assumptions. The depth of euphotic zone varies regionally from 40 m in the Subarctic region to 100 m in the Subtropics. The lowest value of 27 m is evaluated in the region of the continental shelf in the East China Sea.

4. Distributions of nitrogen compounds and chlorophyll-a concentrations in the seas around Japan

Mean values of ammonia, nitrite, nitrate and chlorophyll-a concentrations are shown in

---

* Light intensity (I_z) at given depth (Z) is formulated as follows,

$$I_z = I_0 e^{-kz}$$

where, I_0 is the light intensity at the sea surface. k is an extinction coefficient of the intensity in sea water. If the light intensity at the compensation depth is assumed to be 1% of sea surface illumination, the depth of euphotic zone (Z) defined as the depth from the sea surface to the compensation depth can be estimated by the following equation. $Z = \frac{1}{k} \log_e 100$ k is assessed from the transparency reading by Secchi disk using the following equation (POOLE et al., 1929).

$$k = 1.7/\text{transparency}$$

Then,

$$Z = 2.7 \text{ transparency}$$

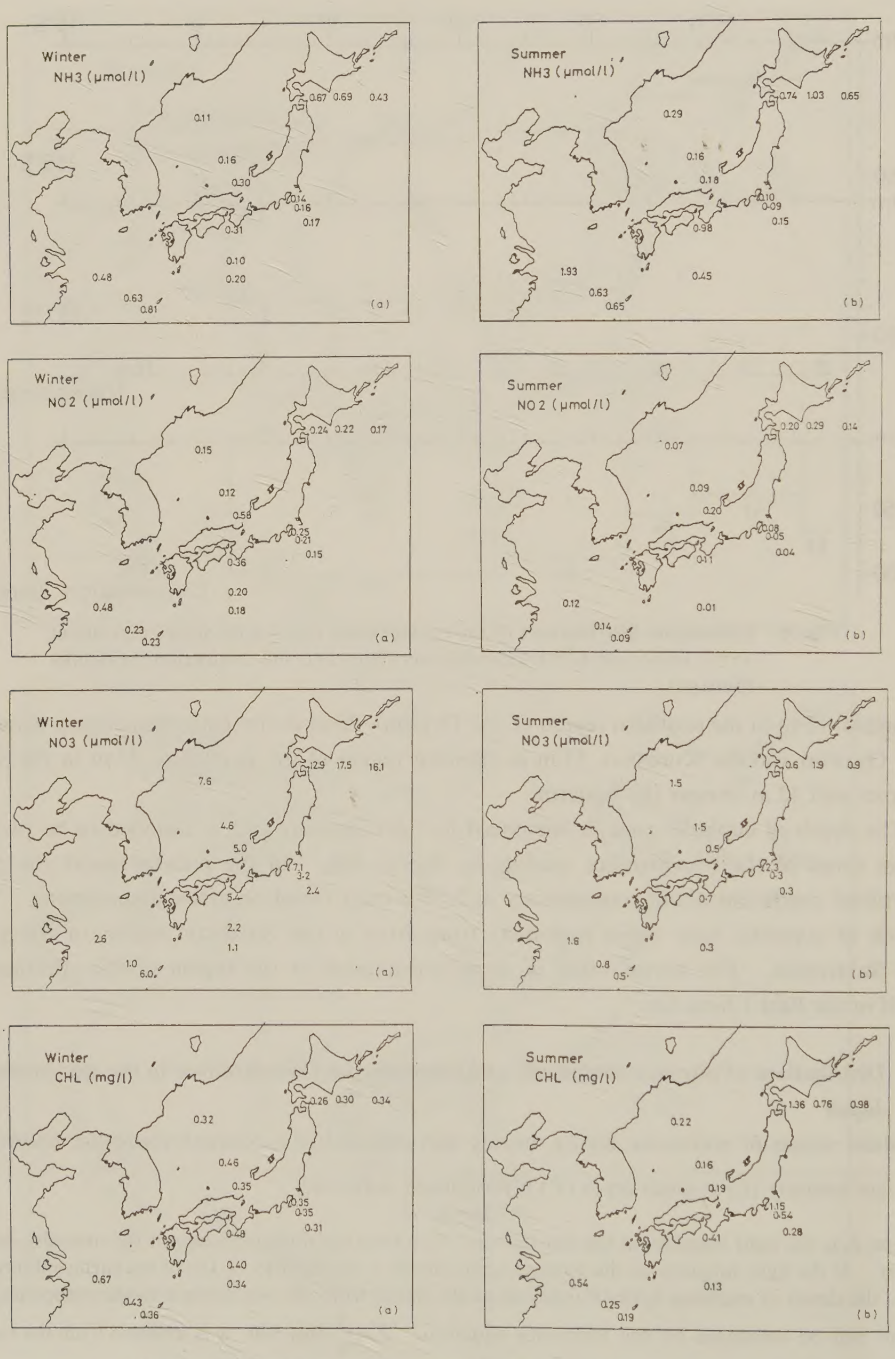

Fig. 5. Mean concentrations (1980–1985) in the euphotic zone of ammonia, nitrite, nitrate and chlorophyll-a in the seas around Japan.

Fig. 5. "Mean" is defined as the mean value for a six-year period (1980–1985) in the euphotic zone in each region as described before.

Ammonia concentrations are relatively high in the East China Sea and off the southern Hokkaido. At the stations far from the east of the Yangtze river and off the Kii channel the ammonia rich water about 1–2 μmol/l are found in summer. The high concentration of ammonia at the coastal areas including the continental shelf in the East China Sea seems to be ascribed to the land drainage.

Set aside the maximum concentration of nitrite near the compensation depth for photosynthesis, small but measurable concentration of nitrite about 0.2 μmol/l appears to be uniformly distributed in winter throughout the euphotic zone. The concentration of nitrite are slightly higher in winter than in summer. It is supposed that surface cooling and mixing during winter markedly weaken the density stratification and lead to high nitrite concentration with a rather uniform vertical distribution.

A difference in the distribution of nitrate between winter and summer is more clear than that in the nitrite distribution. Particularly, nitrate rich waters (12–18 μmol/l) in winter are found at the regions off the southern Hokkaido. It is well known that those regions are active sites of vertical mixing in winter and the nitrate concentrations increase rapidly with depth in the further depth than the compensation depth. It is certain that nitrate rich water in the decomposition layer is brought into the euphotic zone with vertical mixing in winter.

The chlorophyll-a concentration as an index of plankton biomass in the euphotic zone is much higher in summer than in winter at the regions off the southern Hokkaido irrespective of the eutrophy in winter. While, the chlorophyll-a concentration is rather higher in winter than that in summer in the East China Sea and the Japan Sea.

5. Latitudinal distributions of nitrogen compounds and chlorophyll-a concentrations

Distributions of the mean values in the euphotic zone of nitrogen compounds ($NH_3+NO_2+NO_3$) concentration, chlorophyll-a concentration and the water temperature along 155°E meridians are shown in Fig. 6. Those mean values vary regionally corresponding to the current system of the western North Pacific as shown in the lower part in the figure.

In the northern region of the Oyashio, the mean concentration of nitrogen compounds amounts to 24 μmol/l which is about two times as high as the value in the southern region of the Oyashio, but the mean concentration of chlorophyll-a is a half of the value in the southern region of the Oyashio. The mean temperature decreases from 10° to 2°C to the north in the Oyashio.

On the other hand, in the Subtropics, the mean concentrations of nitrogen compounds and chlorophyll-a are lower than 1 μmol/l and 0.1 μg/l, respectively. In this region, a parmanent thermocline which obstructs the vertical transfer of nutrients from deep water exists below the euphotic zone.

It can be said that the biological productivity is limited by the temperature in the northern region of the Oyashio and is limited by the depletion of nitrogen compounds in the Subtropics.

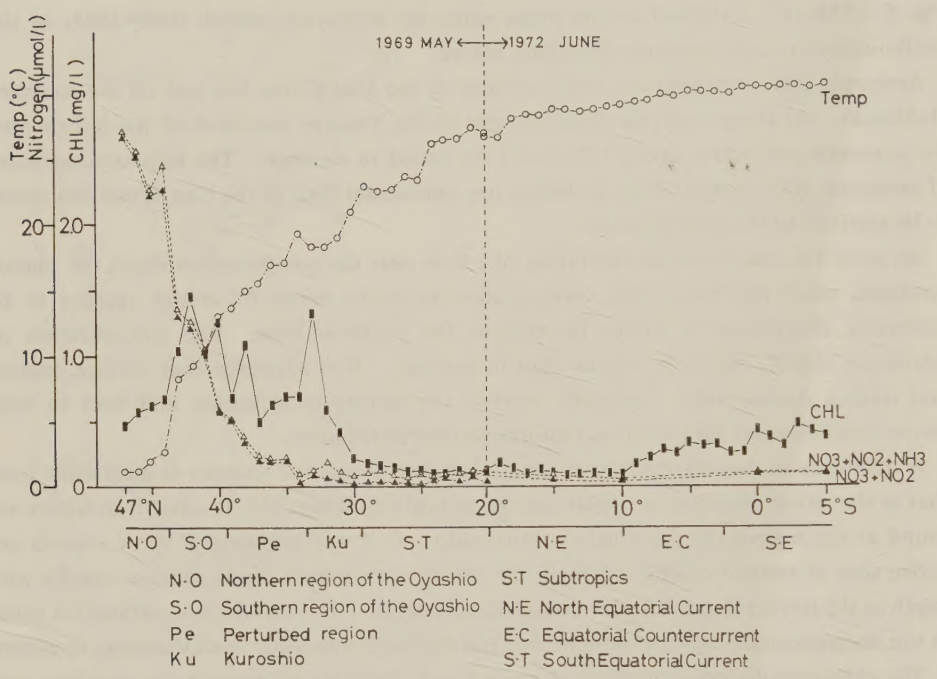

Fig. 6. Latitudinal distributions of the mean values in the euphotic zone of nitrogen compounds and chlorophyll-a concentrations and of the temperature along 155°E meridian.

A rather high concentration of chlorophyll-a exists in the northern region of the Kuroshio. Though it is not clear because of insufficient data, it is assumed that the nutrients must be supplied to the euphotic zone through the mixing of the coastal water and the Kuroshio in the south of Japan.

Near the Equator, the chlorophyll-a concentration is higher than that in the Subtropics. It is well known that this region is active site of upwelling. It is presumed that the water in the decomposition layer is brought into the euphotic zone and shows high biological productivity.

6. Conclusion

To confirm the regional oceanographic features controlling biological production, the distributions of nitrogen compounds and chlorophyll-a concentrations in the euphotic zone in the seas around Japan and along the 155°E meridian are examined.

The ammonia concentration in summer is high in the East China Sea and off the Kii channel under the influence of the land drainage. In the Oyashio region of the southern Hokkaido, it is found that chlorophyll-a concentration is low in winter, though the nitrogen compounds show remarkably high concentrations. The biological productivity seems to be limited by the temperature in the Oyashio region. Both the concentrations of nitrogen

compounds and chlorophyll-a in the euphotic zone are low in the Subtropics. It suggests that biological production is limited by the depletion of nitrogen compounds in this region.

The mutual relations among various forms of concentrations of nitrogen compounds in the euphotic zone has been little clarified as yet. Organic nitrogen compounds play a very significant role with their inorganic compounds for that cycle of nitrogen. The further study using reliable data on organic nitrogen is needed earnestry.

Acknowledgements

The authors wish to acknowledge members of Oceanographical Division of Hakodate, Maizuru, Kobe, Nagasaki Marine Observatories and Japan Meteorological Agency for their help in determination of elements in the present report.

References

POOLE, H. H. and W. R. G. ATKINS (1929): Photo-electric measurements of submarine illumination throughout the year. J. Mar. biol. Ass. U. K., **16**, 297–324.

SAGI, T. (1978): The ratio of nitrate to phosphate in sea water of the Pacific. Oceanogr. Mg., **29**, 23–34.

TAKATANI, Y. (1987): Vertical profile of nutrients in sea water pumped up through a long polyethylene tube. KER Annual Contribution (in Japanese), period 2, vol. 1, 220–225.

有光層における窒素化合物とクロロフィルーa の 分布

角 野 康 二 ・ 鷺 猛

(気象庁海洋気象部)

生物生産は，主として有光層内において行われており，アンモニアや亜硝酸は有光層内で極大層を形成する．一方，酸化分解によって形成される硝酸は，補償深度以深で急激に増加する．そのため窒素化合物の表面付近における海域分布や生物活動を考察するには有光層内における窒素化合物の把握が必要である．

有光層内の分布から補償深度の浅い東シナ海，紀伊水道沖では陸からの窒素化合物の負荷が大きく，生物活動も活発であることが示唆される．しかし，親潮域北方や冬季親潮域においては，窒素化合物が高濃度であるにもかかわらず水温が低いため生物生産が抑えられる．また亜熱帯域や熱帯付近での生物生産は深層からの窒素の補給によってまかなわれていると考えられる．

The Oceanographical Magazine
Vol. 39, Nos. 1-2, pp. 11 to 19, March 1989

Distribution and behavior of bismuth in Tokyo Bay

Jun-ichi OHYAMA
Japan Meteorological Agency
Fumi MARUYAMA
Takamatsu Local Meteorological Observatory
and
Yukiko DOKIYA
Meteorological College

(Received September 27, 1988; Accepted November 18, 1988)

Abstract: The distribution of bismuth in sea-water and sediments in Tokyo Bay has been investigated in order to understand the behavior of the element in the coastal area. Bismuth concentrations in sea-water varied in the range of 0.5 to 2.1 ng/l. At the stations near the central part of the bay, vertical profiles exhibited a mid-depth minima which might be resulted from the inputs of the element at the surface and near the bottom, and from the scavenging throughout the water column. The high contents in surface sediments, ranging from 1.4 to 2.4 μg/g, were observed at the inner half of the bay. It was found that an amount which was higher than 90% of total output of the element was accumulated into sediment, and the mean residence time in the bay water was very short (0.011 years). From the results, bismuth loaded to Tokyo Bay was considered to be transferred rapidly into the sediment.

1. Introduction

Bismuth is one of the elements whose distributions and behavior in sea-water have not been investigated owing to the difficulty in clean handling techniques and in measurements. Recent development in new analytical methods for the element have enabled to determine the concentration of the order of ng/l or less (LEE, 1982; OHYAMA *et al.*, 1987; YOSHIMURA, 1987). These investigators have found the concentrations of the element to be in the range of 0.6 to 3.6 ng/l in the coastal waters. BRULAND (1983) and LEE *et al.* (1985/1986) have suggested from the consideration of the vertical profile in the oceanic water column that bismuth in sea-water is probably present as a hydroxy species and is strongly scavenged by particles. Also, OHYAMA *et al.* (1987) have reported that the distribution of bismuth content in coastal sediment core may serve as an index of anthropogenic activity. However, little other information is available at present on its behavior in oceanic environment.

A coastal area is one of the most important research fields for the study on the behavior of trace elements, because major processes controlling the distributions are found to be remarkably concentrated in this area. The present paper describes the distributions of bismuth in sea-water and core sediments of Tokyo Bay where large amounts of pollutants are introduced through human activities. The behavior of the element in the coastal

environment will be discussed by estimating its residence time and removal rates from the bay.

2. Experimental

2-1 Samples

All samples were collected on the R/V Ryofu Maru cruises of Sept. 1985, and Sept. and Dec. 1986 in Tokyo Bay. The bay has an area of 910 km^2 and the total water volume is 16.0 km^3. Four large rivers (Edo, Arakawa, Sumida and Tama River) discharge into the north western part of the bay. Water exchange between the bay and the open sea occurs only through the bay mouth of 6 km wide. This semi-closed bay is well known as one of the most polluted areas in Japan.

The sampling stations for the sea-water and sediments taken in the present study are shown in Fig. 1. The surface water was directly collected by dipping a Teflon bottle below the surface water while the ship was running. The subsurface sea-water samples were taken with a 10 liters Niskin bottle. These samples were immediately acidified to pH 2 with hydrochloric acid without filtration, and stored in polyethylene bottles which had been precleaned with 6 M HCl. The acidified sea-water was preserved for two months

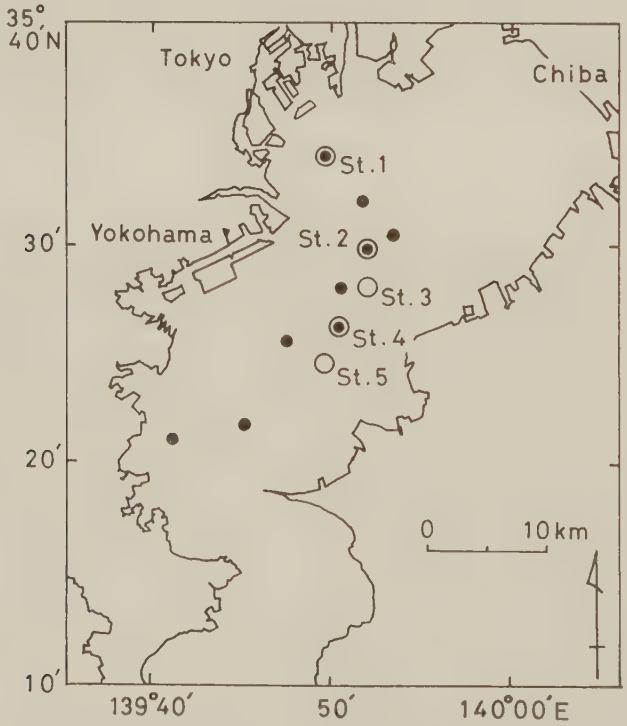

Fig. 1. Sampling stations of sea-water and sediments in Tokyo Bay. ● : surface seawater, ○ : sediment, ◉ : seawater and sediment.

at room temperature in order to dissolve the bismuth from colloidal and/or suspended materials.

Core sediment samples were collected by means of a 1 m gravity corer (5.2 cm polycarbonate I.D. tubu), and they were cut into 5 cm vertical fractions. The interstitial water was removed by a centrifuge for 15 min at 3,000 rpm on board.

2-2 Pretreatment and Analysis

An aliquot of 5 liters of sea-water was used for one analysis. Trace amounts of bismuth in a sample were coprecipitated by the addition of 7.5 ml of 6 M NaOH, and filtered after stirring for 15 min. The precipitate on the filter was dissolved with 6 M HCl just before the measurement. Then, the solution was diluted to make 15 ml solution of 0.4 M HCl.

A 0.5 g oven-dried sample of each sediment fraction was completely digested with HNO_3, $HClO_4$ and HF in Teflon beaker at 200°C. Ultimately, the residue was dissolved in 50 ml of 0.5 M HCl. In the analysis, a given volume of the sample (0.5 to 3.0 ml) was pipetted and diluted to make 15 ml of 0.4 M HCl solution.

A hydride generation—atomic absorption method (Ohyama *et al.*, 1987) was employed for the determination of bismuth. The detection limit of the method was found to be 1 ng, and the precision was 1.5%.

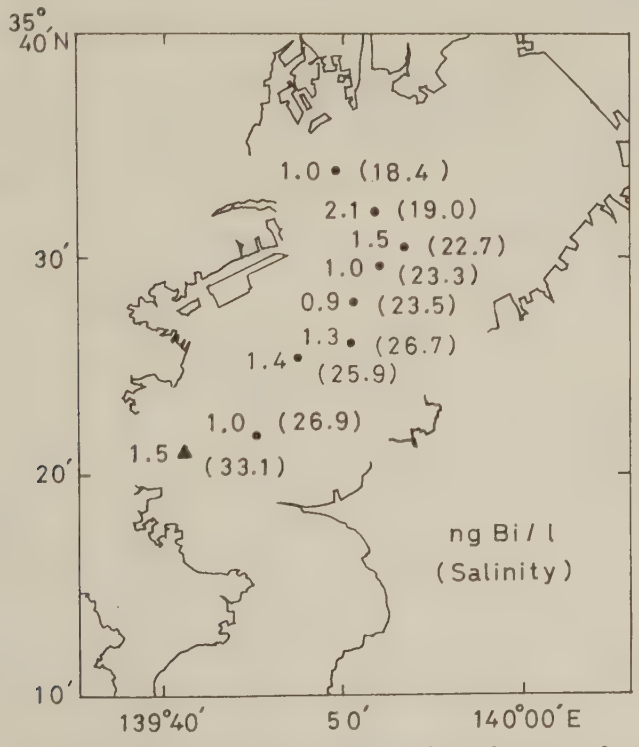

Fig. 2. Geographical distribution of bismuth in the surface water from Tokyo Bay. Salinity is also designated in parentheses. Date of sampling: ●; Sept. 16, 1986, ▲; Dec. 8, 1986.

Sea-water samples were also analyzed for dissolved phosphate by standard auto-analyzer techniques (MIYAO).

3. Results and Discussions

3-1 Distribution of bismuth in sea-water

The horizontal distributions of bismuth and salinity in the surface water of Tokyo Bay are shown in Fig. 2. The concentrations of bismuth ranged from 0.9 to 2.1 ng/l. These values obtained here were similar to those in San Diego Bay and Mission Bay, and were an order of magnitude higher than those in the Pacific Ocean (LEE, 1982). As can be seen in Fig. 2, the distribution of bismuth in the surface waters is not geographically systematic. Furthermore, no correlation can be found between salinity and the concentration of the element. These facts indicate that the distribution of bismuth is not controlled apparently by mixing process with the open sea water. However, more detailed studies on individual distributions of dissolved and particulate forms of the element might be necessary for further discussions, because unfiltered sea-water was used for the analysis in the present study.

Concentration of bismuth and hydrographic data at various depth of the Stations 1, 2 and 4 are summarized in Table 1. The vertical section of salinity observed on Sept. 16 is illustrated in Fig. 3, in which a developed stratification can be seen. This suggests that the distributions of chemical components in the water column are not caused by vertical mixing. On the other hand, the less saline water, which can be attributed to a discharge of the river water, appears in the surface layer. This also shows that the concentrations of chemical components in the surface water are affected by those in the mixing river water.

Table 1 Bismuth concentrations in the water samples from Tokyo Bay

Station number (water depth)	Sampling depth (m)	Bi (ng/l)	Salinity	Water temperature (°C)	O_2 (μM)	PO_4 (μM)
St. 1 (15 m)	0	1.0	18.38	22.8	137	4.85
35°34.0′N	5	0.9	25.47	23.0	31	3.45
139°49.6′E	10	1.1	32.39	22.4	4	3.12
St. 2 (25 m)	0	1.0	23.33	23.1	217	1.24
35°29.7′N	5	1.0	27.05	23.4	109	1.35
139°51.9′E	10	0.5	31.86	21.2	72	1.75
	15	1.5	33.00	20.1	67	1.99
	20	1.5	33.50	19.5	23	2.63
St. 4 (26 m)	0	1.3	26.73	23.4	214	0.74
35°26.0′N	5	1.4	27.65	23.4	176	0.81
139°50.3′E	10	1.7	31.70	21.5	151	0.94
	15	0.7	33.61	20.8	172	1.21
	20	1.2	33.75	20.7	134	1.17
	average	1.3±0.36				

date of sampling: Sept. 16, 1986

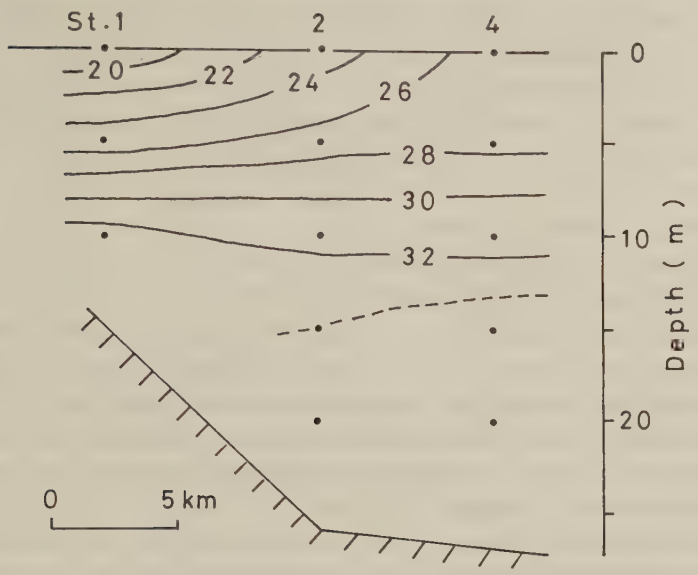

Fig. 3. Vertical section for the distribution of salinity in Tokyo Bay observed on Sept. 16, 1986.

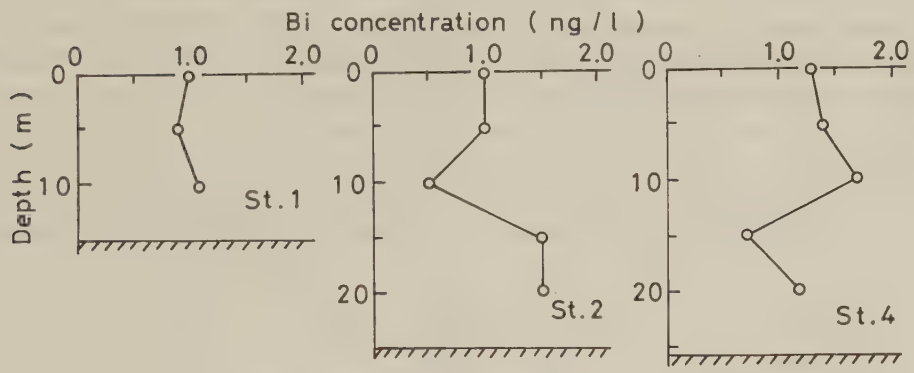

Fig. 4. Vertical profiles of the distribution of bismuth in the Tokyo Bay water on Sept. 16, 1986. Station numbers in the figure correspond to those in Fig. 1.

Vertical profiles of bismuth are shown in Fig. 4. At Station 1 located innermost part of the bay, the concentrations of the element are relatively uniform in the water column, regardless of the abrupt change of dissolved oxygen or salinity with depth. In contrast, the profiles at Stations 2 and 4 show mid-depth minima at 10 and 15 m depth, respectively. The vertical profiles are known to be resulted from the inputs of the element at the surface and near the bottom layer, and from the scavenging throughout the water column. Similar profiles were reported for some trace metals in same area of the bay (AKAGI and HARAGUCHI, 1984). High concentration of bismuth at the surface might be caused from some anthropogenic loads derived through the river water and/or the atmospheric deposition. This

view is supported by the fact that the concentration in the bay water is an order of magnitude higher than that in the open sea water. The processes leading to the bottom enrichment can be considered to be derived either from the dissolution of bismuth from settling particles or from the release of the element from bottom sediments. However, the processes are not completely clear yet, because too little information in this connection for bismuth has been available.

3-2 Distribution of bismuth in sediments

Figure 5 shows the distributions of bismuth in sediment cores at Stations 1, 3 and 5; the northern, the central and the southern part of the bay. As seen in the figure, the bismuth contents were relatively constant below 20 cm from the surface of the cores at Stations 3 and 5 ranging from 0.15 to 0.33 μg/g. It can be considered that the relatively constant contents found in this work may represent the background levels in the sediment of the bay, judging from the contents of the element in the surface sediments from the Pacific Ocean and in the pre-1900 sediment from Narragansett Bay, 0.10 and 0.27 μg/g respectively (Lee, 1982).

In the upper layer, abrupt changes in content are observed. In particular, the maximum contents of bismuth at Stations 1 and 3 were 4.6 and 2.4 μg/g, and they were enriched relative to the contents of the lowest layer by the factor 11 and 8.0 respectively. The high enrichment ratio seems to reflect an increase in the recent anthropogenic load.

Bismuth contents in the uppermost 5 cm layer are listed in Table 2. The average content is calculated to be 1.4 μg/g. The higher bismuth contents than the average value are found in the northern half parts of the bay. The distribution describes that bismuth loaded to

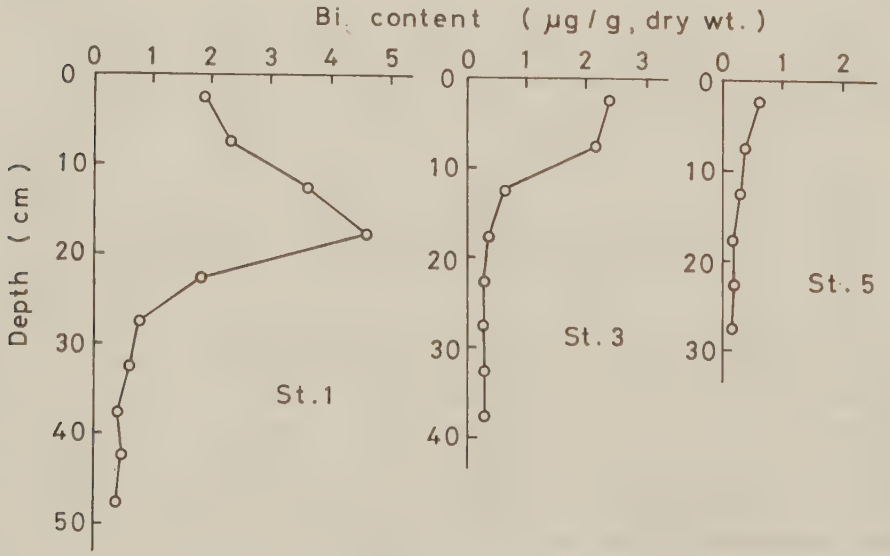

Fig. 5. Vertical profiles of the distribution of bismuth in sediment cores from Tokyo Bay. Station numbers in the figure correspond to those in Fig. 1.

Table 2 Bismuth contents in surface sediments (0–5 cm layer) from Tokyo Bay

Station number	Location	Bi content (μg/g dry wt.)
St. 1:	35°34.0′N, 139°49.6′E	1.9
St. 2:	35°29.7′N, 139°51.9′E	1.4
St. 3:	35°28.6′N, 139°51.6′E	2.4
St. 4:	35°26.0′N, 139°50.3′E	0.7
St. 5:	35°24.8′N, 139°49.5′E	0.6
	average	1.4

sea-water was removed predominantly in the inner parts of the bay at present.

3-3 Behavior of bismuth in Tokyo Bay

A simple box model analysis is carried out in order to understand the behavior of bismuth in Tokyo Bay. In the approach adopted here, it is assumed that the bay can be represented as a box which is well mixed and considered to be in a steady state with respect to the water and chemical components. This assumption describes that the flux supplied to the bay water is equal to that removed from the water. In addition, bismuth in the bay water is considered to be removed through the processes of the accumulation into sediment and of the outflow through the water exchange between the bay and the open ocean. A simple model expressing these processes is shown in Fig. 6.

The sedimentary load of bismuth from sea-water is calculated to be 1.7 ton/yr, by using the average content in the surface sediments (1.4 μg/g) and mean sedimentation rate in Tokyo Bay of 1.2×10^6 ton/yr reported by MATSUMOTO (1983). A removal rate of bismuth to the open ocean through the sea-water exchange, 0.16 ton/yr, is estimated by the average concentration in the water (1.3 ng/l) and the annual mean value of the outflow to the open ocean of 124 km^3/yr (UNOKI and KISHINO, 1977). That is to say, an amount which is higher than 90% of bismuth supplied to Tokyo Bay is accumulated into sediment. This

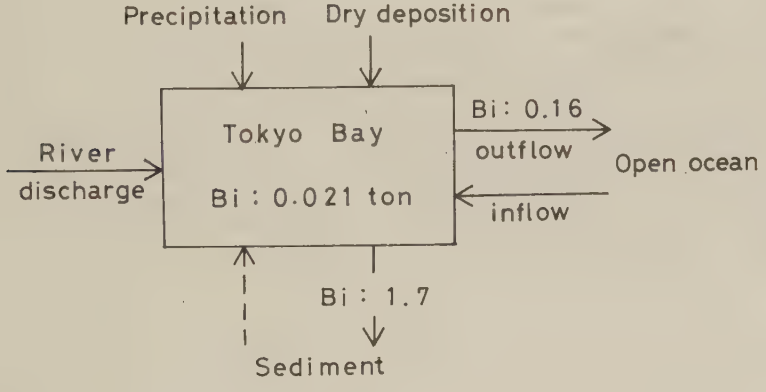

Fig. 6. Schematic diagram of box model for the budget of bismuth in Tokyo Bay. Fluxes are shown in ton/year.

result suggests that the scavenging to the sediment, which may be transported with particles, contributes significantly to the present geochemical cycle of the element in the bay.

A mean residence time of bismuth in Tokyo Bay is given, in years, by dividing total amount of the element in the water by the annual removal rate from the bay, when steady state can be assumed with respect to the component. The total amount is calculated to be 0.021 ton as the product of the average concentration of the element and the water volume of the bay (16.0 km^3). The annual amount carried away from the bay is estimated (1.9 ton/yr) as the sum of the removal rate of the accumulation into sediment and of the outflow to the open ocean. Therefore, the mean residence time is calculated to be about 0.011 years. The value for bismuth is smaller not only than the mean residence time of the water in Tokyo Bay (0.13 years) but also than those of other heavy metals (Pb; 0.013 years, Cu; 0.051 years, Hg; 0.083 years) showed by MATSUMOTO (1987). This small value describes the very rapid scavenging of bismuth from the sea-water. The cause might be attributed to the existence of the element as a hydroxy species which is geochemically reactive.

Acknowledgement

The authors wish to express their sincere thanks to the captain H. YASUDA, and the crew of the R/V Ryofu Maru of Japan Meteorological Agency for their kind help in sampling.

References

AKAGI, T, and H. HARAGUCHI (1984): Distributions and behaviors of trace heavy metals in the Tama River Estuary and Tokyo Bay., *Chikyuukagaku*, **18**, 81–88.

BRULAND, K. W. (1983): Trace elements in sea-water., Chemical Oceanography No. 8, Academic Press, 187–188.

LEE, D. S. (1982): Determination of bismuth in environmental samples by flameless atomic absorption spectrometry with hydride generation., *Anal. Chem.*, **54**, 1682–1689.

LEE, D. S., J. M. EDMOND and K. W. BRULAND (1985/1986): Bismuth in the Atlantic and North Pacific: a natural analogue to plutonium and lead?, *Earth Planet. Sci. Lett.*, **76**, 254–262.

MATSUMOTO, E. (1983): The sedimentary environment in the Tokyo Bay., *Chikyuukagaku*, **17**, 27–32.

MATSUMOTO, E. (1987): Material balance in Tokyo Bay., Proceedings of the 1987 annual meeting of the Geochemical Society of Japan, Abstr. 138–139.

MIYAO, T.: Determination of nutrient salts in sea water by auto-analyzer system., to be published in *Weather Service Bull.* (Japan Meteorological Agency).

OHYAMA, J., F. MARUYAMA and Y. DOKIYA (1987): Determination of bismuth in environmental samples by hydride generation-atomic absorption spectrometry., *Anal. Sci.*, **3**, 413–416.

UNOKI, S., and M. KISHINO (1977): Oceanographic conditions and water exchange in Tokyo Bay., Institute of Physical and Chemical Research. Tech. Rep. No. 1, pp. 89.

YOSHIMURA, K. (1987): On-line concentration and flow analysis of trace amounts of bismuth with anion-exchange absorptiometry., *Bunseki Kagaku*, **36**, 656–661.

東京湾におけるビスマスの分布と挙動

大　山　準　一
（気象庁海洋気象部）
丸　山　　文
（高松地方気象台）
土器屋　由紀子
（気象大学校）

沿岸域における ビスマスの挙動を 調べる目的で，東京湾の海水 及び堆積物中の濃度分布 を調べた．海水中のビスマス濃度は 0.5～2.1 ng/l の範囲で存在し，東京湾中央部での海水中の鉛直分布は中層で極小をとることが見いだされた．このことから，ビスマスは海水中の各層を通じて除去を受けている一方で，表層と深層で付加過程が存在することが推論された．表層堆積物中の濃度分布は，東京湾の湾奥部で 1.4～2.4 μg/g の高い分布を示した．得られた値を用いた見積りによって，東京湾ではこの元素の年間流出量の 90% 以上が堆積物中に畜積すること及び湾内水における平均滞留時間が 0.011 年ときわめて短いことから，東京湾へ負荷されたビスマスはすみやかに堆積物中に移行することが示された．

The Oceanographical Magazine
Vol. 39, Nos. 1-2, pp. 21 to 42, March 1989

Numerical Forecast of Storm Surges on Real Time Basis

Tatsuo KONISHI
Japan Meteorological Agency

(Received November 20, 1988; Accepted December 2, 1988)

Abstract: A dynamical-numerical model for storm surge forecast on real time basis is presented. The traditional equations for the simulation of storm surges are used for water motion in the method. Pressure distribution in a typhoon is expressed by the FUJITA's formula and the wind distribution by the MIYAZAKI's formulation. The number of the parameters which should be determined on real time for use of the formula in this model is limited to six, such as the longitude and latitude of initial typhoon position, the speed and the direction of the typhoon movement, the minimum pressure and the radius of the maximum wind and the others are supposed to be constants for all cases.

The past five typhoons which caused big storm surges in Tokyo Bay are chosen to verify this model and the results show that the model can predict the peak of storm surge within the error margin of 10%, if the maximum wind and minimum pressure are forecast correctly.

In the calculation, a new type of open boundary condition is proposed to reduce the computational noise and to simulate the inverted-barometric balance properly at a deep open ocean.

1. Introduction

Until now, the quantitative forecast of storm surges on real time basis has been performed by the empirical formula (Japan Meteorological Agency (1988)). In this formula, the peak surge, which is the most important quantity, can be predicted very simply with tolerable accuracy. However the method has the defects that need a large number of observations to establish a meaningful correlation between observed storm surges and meteorological elements for prediction and the method can not forecast the time variation of storm surges.

Numerical simulations of the past storm surges were extensively conducted for important bays from the viewpoint of disaster prevention by MIYAZAKI *et al.* (1962) and UNOKI *et al.* (1964). The capacity and the speed of the computer was not enough and the forecast of the typhoon course was not accurate at that time and then the application of the method has been limited to estimation of the design tide level to construct the facilities of disaster prevention such as coastal levees and tide gates in coastal area (Tokyo Metropolitan Government (1986)).

In this paper, a dynamical-numerical method of storm surge forecast on real time basis is presented. This is basically based on the conventional models of storm surge simulation, but a new condition is used for open sea condition to satisfy the following two conditions. One is to reduce the computational noise in the domain and another is to simulate the inverted-barometric condition at open ocean properly. The five typhoons, which attacked Tokyo bay in the past and caused big surges, were chosen to verify this model and the

results show that this numerical model can predict storm surges more accurately than empirical models, if the maximum wind and the minimum pressure of the typhoon are predicted correctly.

2. Fundamental Equations and Boundary Conditions

UNOKI *et al.* (1964) performed the scale analysis to ascertain the relative importance of the various terms of the Navier Stokes equations. They ignored the terms with square order of small parameters and obtain the following equations,

$$\frac{\partial M}{\partial t}-fN=-g(D+\zeta)\frac{\partial(\zeta-\zeta_0)}{\partial x}+\frac{T_{sx}}{\rho_w}-\frac{T_{bx}}{\rho_w}-\varepsilon(D+\zeta)\left\{\frac{\partial u^2}{\partial x}+\frac{\partial uv}{\partial y}\right\}$$

$$\frac{\partial N}{\partial t}+fM=-g(D+\zeta)\frac{\partial(\zeta-\zeta_0)}{\partial y}+\frac{T_{sy}}{\rho_w}-\frac{T_{by}}{\rho_w}-\varepsilon(D+\zeta)\left\{\frac{\partial uv}{\partial x}+\frac{\partial v^2}{\partial y}\right\}$$

$$\frac{\partial \zeta}{\partial t}=-\frac{\partial M}{\partial x}-\frac{\partial N}{\partial y}$$

where M and N are the horizontal transports, $M=u(D+\zeta)$ and $N=v(D+\zeta)$, in the x and y directions respectively, u and v are the mean velocities of the vertical water column in the x and y directions, ε is the correction factor for the flow profile in a water, ζ is water level above mean sea level, f is the Coriolis parameter, g is gravity, ρ_w is the uniform density of water, t is time, ζ_0 is the water head corresponding to the difference of atmospheric pressure from the periphery, D is water depth, T_{sx} and T_{sy} are the x and y components of wind stress, T_{bx} and T_{by} are the x and y components of the bottom friction. Among the terms of the above equations, terms such as $g\zeta\partial(\zeta-\zeta_0)/\partial x$ and the last advection terms are smaller than others, but the former terms have the order ζ/D and they may become large near the coast and we keep it. As a result, we use the following equations as the fundamental equations,

$$\frac{\partial M}{\partial t}-fN=-g(D+\zeta)\frac{\partial(\zeta-\zeta_0)}{\partial x}+\frac{T_{sx}}{\rho_w}-\frac{T_{bx}}{\rho_w}$$

$$\frac{\partial N}{\partial t}+fM=-g(D+\zeta)\frac{\partial(\zeta-\zeta_0)}{\partial y}+\frac{T_{sy}}{\rho_w}-\frac{T_{by}}{\rho_w} \qquad (1)$$

$$\frac{\partial \zeta}{\partial t}=-\frac{\partial M}{\partial x}-\frac{\partial N}{\partial y}$$

The equations are transformed to difference equations and the numerical integration of the above equations gives the forecast of storm surges, ζ and transports M and N. Leap frog method is used for the time integration. Grid interval of space is 1.9 km and the time interval is 5 seconds.

Wind stresses and bottom stresses are supposed to be proportional to the square of wind velocity and the square of the mean flow velocity respectively as follows,

$$\boldsymbol{T}_s=\rho_a C_d \mid \boldsymbol{W} \mid \cdot \boldsymbol{W}$$

$$\boldsymbol{T}_b=\rho_w C_{dw} \mid \boldsymbol{U} \mid \cdot \boldsymbol{U} \qquad (2)$$

where ρ_a is the air density, $\boldsymbol{W}$ is the wind vector, $\boldsymbol{U}$ is the mean flow vector, C_d and C_{dw}

are drag coefficients for air-sea boundary and sea-bottom boundary respectively. In our calculation, C_{dw} is 2.6×10^{-3} as same as convention. Though there are some kinds of formula about C_d, we use 3.5×10^{-3} as the drag coefficient in this calculation because Konishi *et al.* (1985) could obtain good agreements between observation and calculation with the same magnitude as 3.5×10^{-3}.

Computations are performed in the region as shown in Fig. 1. Only the storm surge component is calculated and the component of astronomical tide is not included in this calculation because the interaction between astronomical tide and storm surges may be weak in Tokyo Bay.

Boundary condition between land and sea is that there is no normal component of the flow across the boundary. Boundary conditions at the open sea may be considered as

Fig. 1. Computed region and selected stations for output with depth distribution.
1: Tokyo, 2: Chiba, 3: Yokohama, 4: Yokosuka, 5: Okada, 6: Mera, 7: Kisarazu, 8: Ito, 9: Katsuura, 10: Oiso, 11: Funabashi.

follows. First, the following conventional condition was used,

$$\zeta=\zeta_0 \tag{3}$$

but it caused a prominent oscillation in the calculated results, though it did not lead an instability. The period of the oscillation showed that the source of it was due to the reflection of the computed noise at the open boundary. The open boundary condition was changed to the so-called radiation condition, which supposes only outwards wave at the open boundary. The condition is defined as the following form,

$$M=\pm\sqrt{gD}\cdot\zeta$$

whose sign is assigned to the each open boundary according to the direction of the advance of outwards wave. This result did not cause the above mentioned oscillation, on the other hand the water level generally decreases, especially at the coast facing on an open ocean. This is because the external forces acting in the region are not incorporated into the boundary condition. The pressure in the computed domain is forced to be low because of the typhoon, which tends to raise sea level constantly, and the radiation condition make the flow outwards corresponding to the sea level gradient at the boundary. This may be the reason why the water level decreases due to the radiation condition.

The conventional condition of equation (3) is reasonable referring to the observed results at the tidal stations of the open coast, but as mentioned above, it induces an oscillation. And then we made a following compromised condition,

$$M=\pm\sqrt{gD}\,(\zeta-\zeta_0). \tag{4}$$

This condition means that the excess rise or depression from the inverted barometric balance satisfies the radiation condition, which we call as radiative-barometric condition below. The comparison among the computed results with the three kinds of boundary conditions are shown in Figs. 2.1 and 2.2. The result with radiative-barometric condition shows the same sea level rise as the result with the conventional condition and rather suppresses oscillation. We determined the use of the radiative-barometric condition in the following calculation.

3. Typhoon model

Though we can use the products of numerical weather forecasts for the typhoon model of the storm surge calculation, as the first step, we apply the conventional axi-symmetric typhoon model for the calculation in this paper. Pressure distribution in a typhoon is expressed by the FUJITA's formula,

$$p=p_\infty-\frac{dp}{\sqrt{1+(r/r_0)^2}} \tag{5}$$

In the formula, p_∞ is the peripheral pressure of the typhoon, which we fix as 1010 mb in the below calculation, dp is the depression of the central pressure, r is the distance from the center of the typhoon, and r_0 is the empirical constant. For the wind distribution $\boldsymbol{W}$, Miyazaki's formulation,

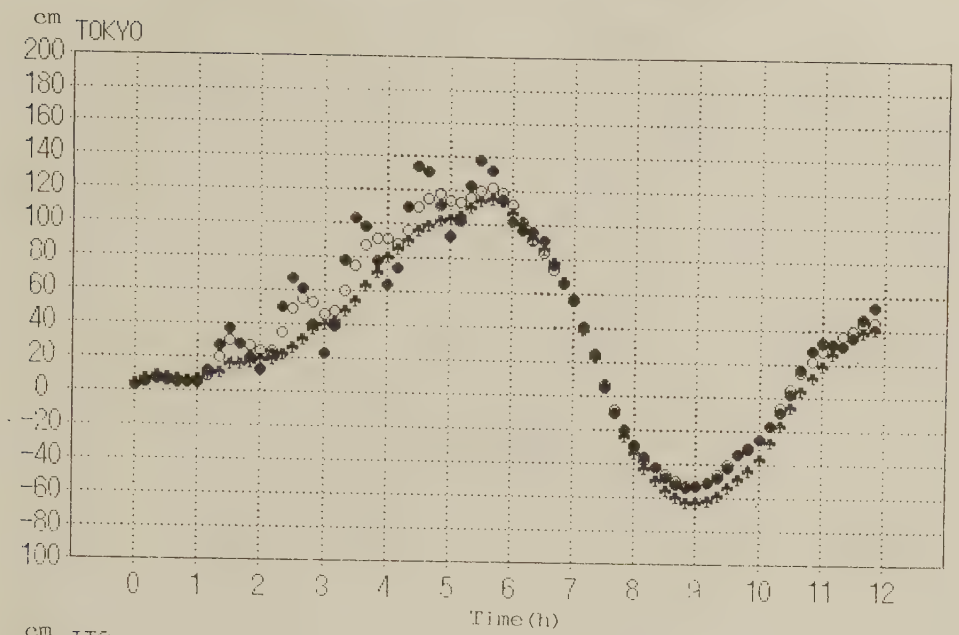

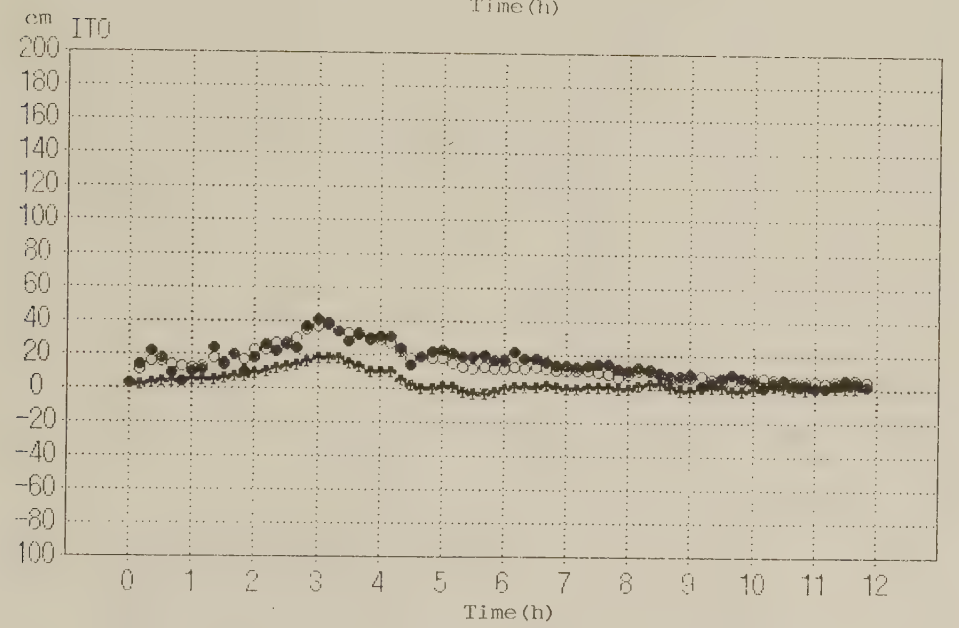

Fig. 2.1. Variation of computed storm surges at Tokyo due to the different boundary conditions at open boundary in case of typhoon 8506. Solid circles: the conventional inverted barometric condition, Clubs: radiation condition, Open circles: radiative-barometric condition. (upper)

Fig. 2.2. Same as Fig. 2.1, but for Ito. (lower)

$$\boldsymbol{W}=C_1\cdot\boldsymbol{G}+C_2\cdot\boldsymbol{C}exp\left(-\frac{\pi r}{r_c}\right) \tag{6}$$

is used, where $\boldsymbol{G}$ is the gradient wind, $\boldsymbol{C}$ is the movement velocity of the typhoon, r_c is the attenuation factor of the general wind towards radial direction, which we fix as 500 km. Magnitudes of these parameters have been chosen so as to be consistent between the computed values and observed values. We suppose the filing of the results calculated in many different cases of typhoons as one of the applications of this numerical model. In order to reduce the cases that we should compute beforehand, we want to reduce the parameters for expressing meteorological fields as less as possible. Therefore, we suppose the three parameters as follows, $c_1=0.6$, $c_2=6/7$, inflow angle of wind is 30° in all computed cases. Numbers of remained parameters determining the distribution of pressure and wind are six, the initial position of a typhoon (tye0, tyn0), the speed and the direction of movement (cvel, cdir), the central pressure of the typhoon, P_0, and the radius of maximum wind, r_0. In order to verify the method, these parameters are determined as follows. First, the positions of the typhoon near the Tokyo Bay, the speed and the direction of the movement are determined. Longitudes of the positions of the typhoons around 33°N are obtained by the extraporation with the above-determined parameters. The tracks of the typhoons selected for verification are shown from Figs. 3.1 to 3.5. These typhoons caused big surges in Tokyo Bay in the past as shown from Figs. 5.1 to 5.5 and Tokyo Bay is very vulnerable for these typical courses of typhoons. In Figs. 3, solid circles are observed centers of the typhoons and open circles are hourly centers supposed in the calculation. The central pressure is determined by the average of observed values from the landing to the nearest approach of the typhoon. Subsidiary computation about 6 hours are performed in order to avoid the fictitious oscillation due to the step-wise forcing. The characteristics of the oscillation are discussed in Section 6. Examples of the oscillations are found from 0 to 5 o'clock in Figs. 6.1 and 6.2. The oscillation seems to attenuate for about three periods of the wave and we can avoid the noise in major surge with the forerunning computation.

Only the remained parameter to be specified is the radius of maximum wind r_0. If a magnitude would be assigned to r_0, the time series of wind and pressure values will be calculated at an arbitrary point. The most proper r_0 is determined by fitting the time series to the observed or forecasted maximum wind and minimum pressure. Only the case of T8506 is discussed below.

Upper graph of Fig. 4 shows the comparison between observed pressures, which is indicated by the symbols of solid circles, and calculated ones which is indicated by numerals in case of T8506. The lower of Fig. 4 shows the comparison between the observed wind speed and the calculated. Numerals in the figure indicate the magnitudes of r_0. The numeral, "1", means $r_0=40$ km, 2 means $r_0=60$ km, 3 means $r_0=80$ km, 4 means $r_0=100$ km, 5 means $r_0=120$ km. The variation of observed atmospheric pressure is similar to the variation of calculated results by $r_0=80$ km or $r_0=100$ km, on the other hand, that of wind speed is similar to the result of $r_0=60$ km. The wind stress is the most effective for storm surges and 60 km is chosen for r_0. Thus, it is difficult to reconcile the calculated

Fig. 3.1. Track of the typhoon 8506. Solid circles are observed positions of the typhoon, which are shown 6 hourly. Open circles are computed one, which are shown hourly. The most southern open circle is placed near 33°N. (upper)

Fig. 3.2. Track of the typhoon 8218. (lower)

Fig. 3.3. Track of the typhoon 7920. (upper)

Fig. 3.4. Track of the typhoon Kitty. The observed typhoon centers are shown 3 hourly. (lower)

Fig. 3.5. Track of the typhoon T6. The observed typhoon centers are shown hourly.

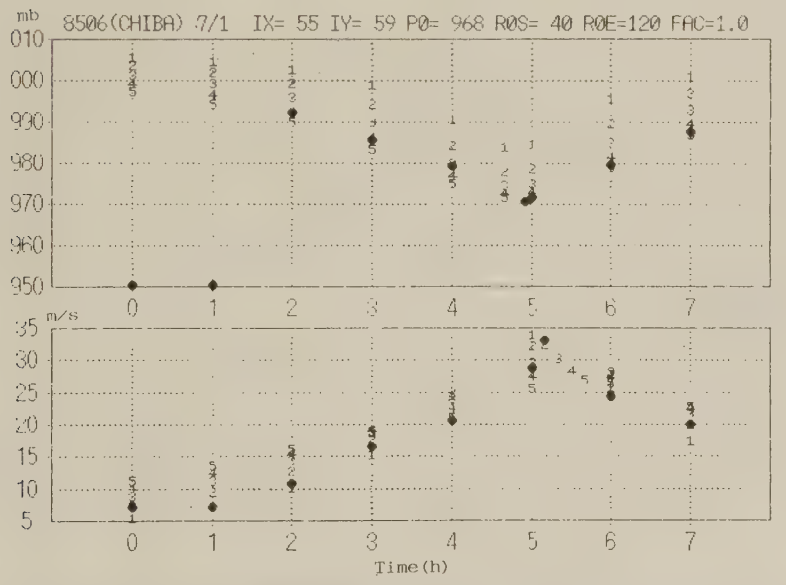

Fig. 4. Graph for determining r_0 in case of T8506. Upper one is the variation of atmospheric pressure and solid circles are observed values. Numerals indicate the different magnitude of r_0. Lower one is the variation of wind speed. IX and IY are the grid numbers in X and Y direction. See the text about the details.

results with observed results. We could choose the different r_0's as the variation of pressure and the variation of wind for the computation of storm surges, however, considering the operation of the model on real time basis, one more parameter increases to be determined and then the cases, which we must compute beforehand, increase greatly, if we would file on computed results to use in real time operation. In our case, only one r_0 is chosen for computation.

The r_0's of remaining cases are also determined similarly.

5. Results of simulated storm surges

The results applied the above method for five cases of the typhoons are as follows.

Case of T8506 (see Fig. 5.1)

Overall feature of the observed storm surges is well-simulated with this method in case of T8506, though the secondary undulations at Tokyo does not appear in the calculation and the calculated result at Chiba is higher than observed results. Calculated results at Yokohama are less than observed one, on the other hand the agreement at Yokosuka is very good.

Case of T8218 (Fig. 5.2)

Generally speaking, the agreement between observation and calculation is rather good, except the time of the peak surge. The tidal station at Chiba is out of operation.

Case of the T7920 (Fig. 5.3)

The peak surges observed at Tokyo and Chiba are nearly equal to the respective observed values. But the calculation does not simulate the forerunner stage well. Also, the calculated peak surge appears earlier. Calculated residuals at Yokohama and Yokosuka are both lower than their respective observed values. Differences are mainly due to the disagreement about the winds. T7920 went through far west from the Tokyo Bay and spatial pressure distribution is modified to be similar to the shape of "pan". The edge of the pan passed over the Tokyo Bay and strong wind was observed in Kanto area. The pan-shaped variation of pressure hardly be expressed by the Fujita's formula and the accuracy of the simulation of meteorological factors is not high.

Case of Typhoon Kitty (Fig. 5.4)

Peak surges at Tokyo are well-simulated but otherwise are not so good.

Case of Typhoon T6 (Fig. 5.5)

The calculated time and the height of the peak surge are different from observation. As was seen in Fig. 3.5, this typhoon doesn't move at a constant speed, on the contrary in the numerical model it was forced to a constant speed. As a result, above-mentioned disagreement may be caused by the improper supposition of the typhoon movements.

6. The variation of predicted storm surges with selected r_0

As seen in the previous section, there is an ambiguity in determining of r_0 and we must check the magnitude of errors due to the selection of different r_0. The storm surge calculated under various r_0 are shown in Figs. 6.1 and 6.2. for T8506. The magnitudes of r_0 range from 20 km to 100 km at intervals of 20 km. In these cases, the beginning

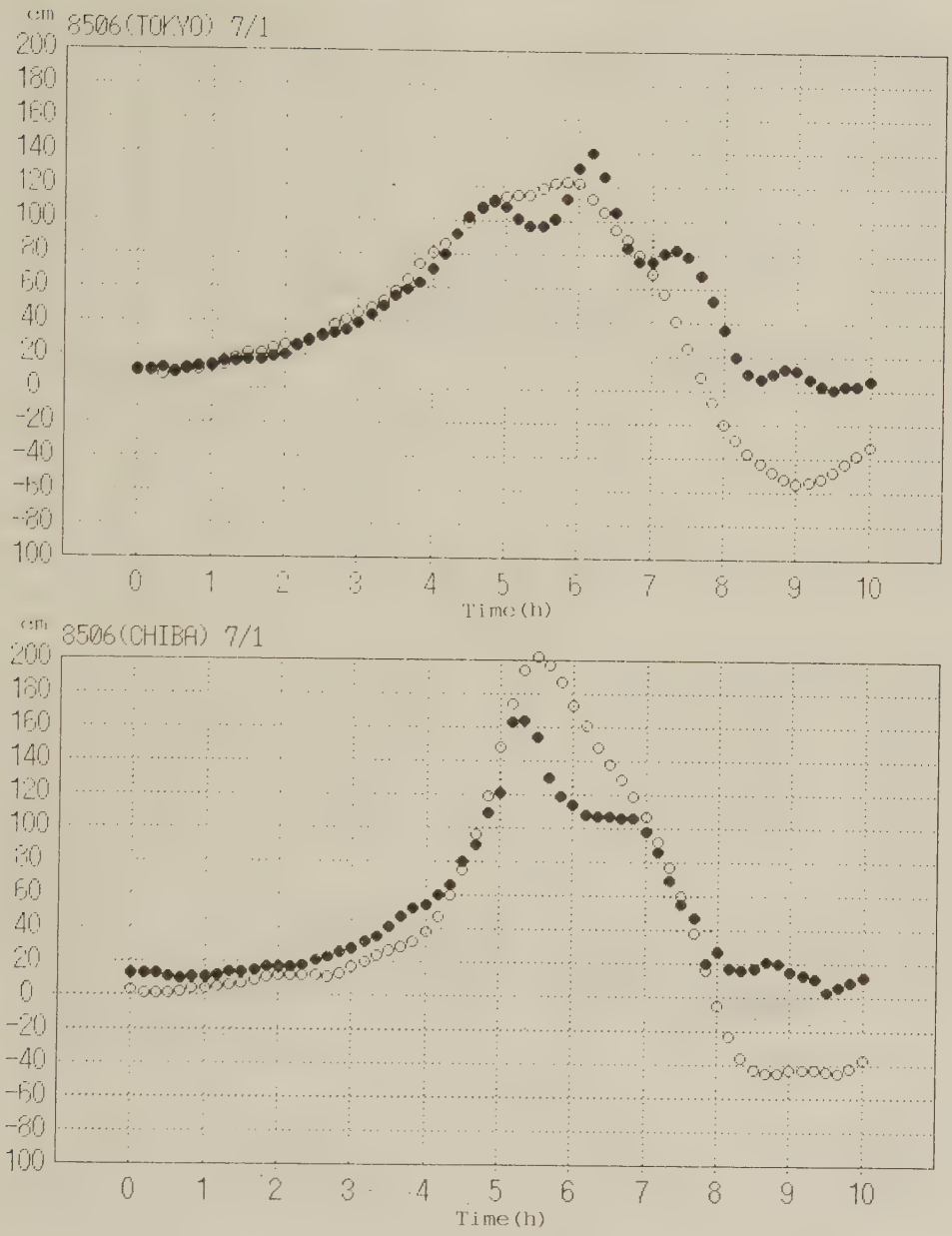

Fig. 5.1.1. Comparison between observed storm surges (solid circles) and computed storm surges (open circles) at Tokyo in case of T8506. (upper)

Fig. 5.1.2. Same as Fig. 5.1.1, but the results at Chiba. (lower)

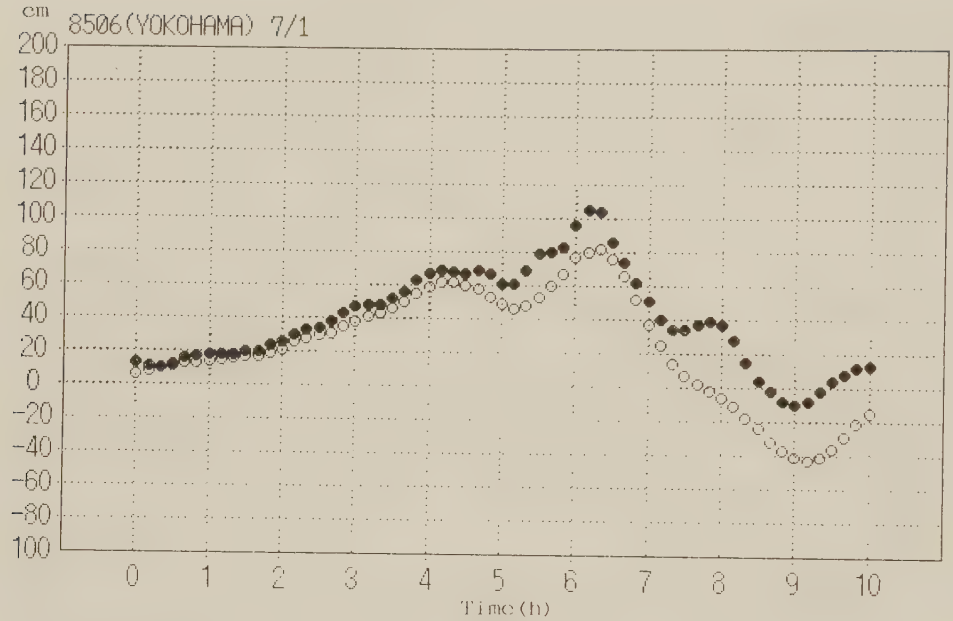

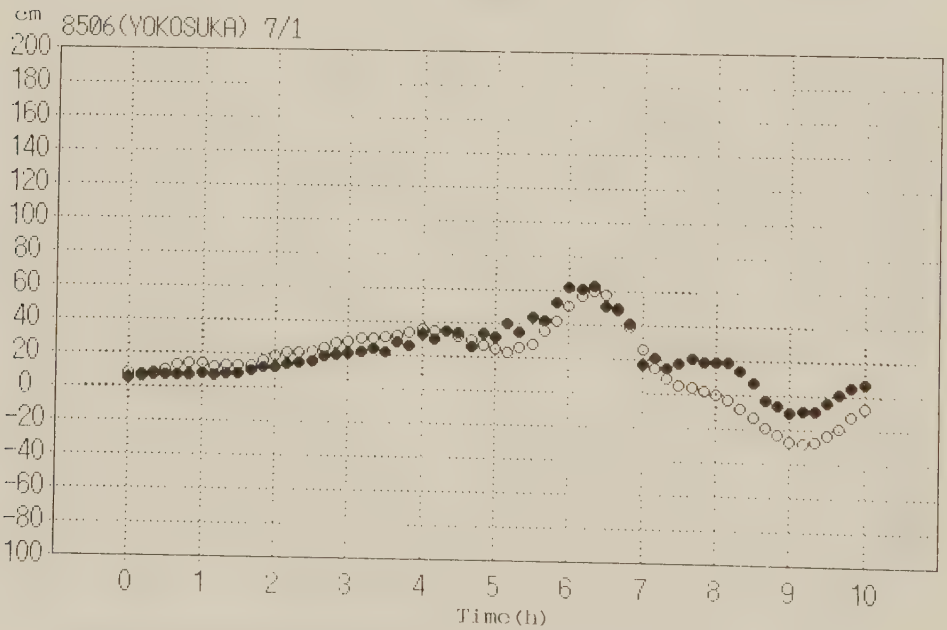

Fig. 5.1.3. Same as Fig. 5.1.1, but the results at Yokohama. (upper)

Fig. 5.1.4. Same as Fig. 5.1.1, but the results at Yokosuka. (lower)

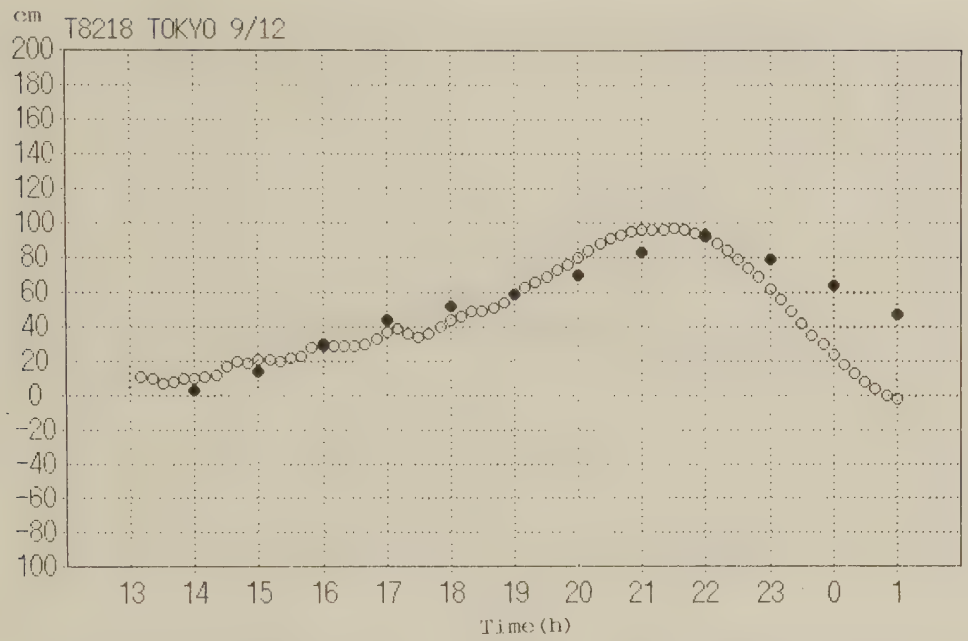

Fig. 5.2.1. Same as Fig. 5.1.1, but the results at Tokyo in case of T8218

time of the calculation is at 0 o'clock. Fig. 4 shows that the maximum wind speed occurs at the r_0 of 40 km and the larger r_0 leads the smaller maximum wind speed.

The maximum storm surge varies with the same manner as the maximum winds. The maximum difference between the peak surges is about 30 cm, and we must anticipate the errors of the peak surge within plus or minus 10 cm, if we select the different r_0 of ± 20 km from the optimum value.

As seen in the figures, large r_0 yields notable oscillations in the earlier period. This reason is considered as follows. Fig. 4 shows that a larger r_0 gives a bigger initial wind speed and also the larger r_0 gives a lower initial pressure, and then the step-like forcing to the Tokyo Bay induces overshoot phenomena and remarkable oscillations.

In order to avoid the occurrence of the phenomena, we started the calculation 6 hours before the first time when we want to obtain the results.

In case that r_0 is equal to 20 km, there is a noticeable oscillation around the peak surge, whose period is a little smaller than observed one, but the characteristics is very similar to the observed oscillations as seen in Fig. 5.1. The reason why the remarkable oscillation occurs in this case may be as same as that of above-mentioned initial oscillation. As the typhoon approaches to the Tokyo Bay, the wind speed increases rapidly in case of small r_0 and sudden increase of wind speed is effective for the cause of the oscillation.

The strong wind continues to blow for a comparatively long time in case of large r_0 after the passing of the typhoon and the case yields to the bigger storm surges than the case of small r_0.

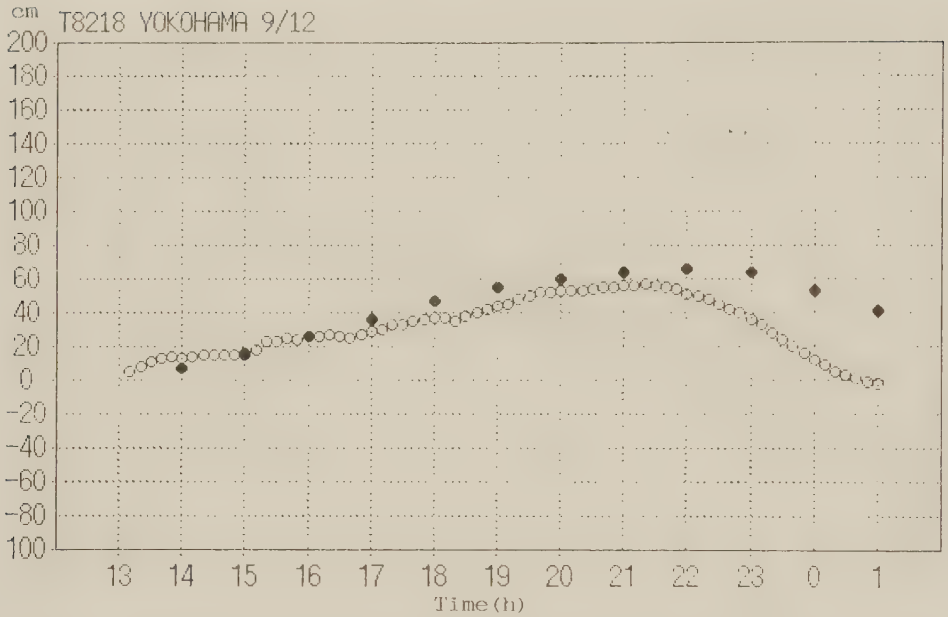

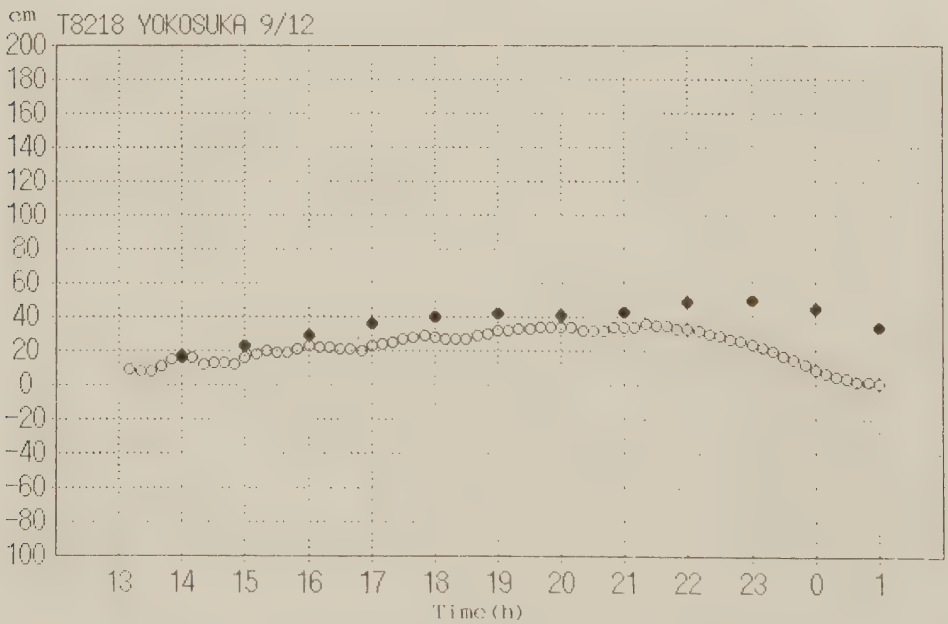

Fig. 5.2.2. Same as Fig. 5.2.1, but the results at Yokohama. (upper)

Fig. 5.2.3. Same as Fig. 5.2.1, but the results at Yokosuka. (lower)

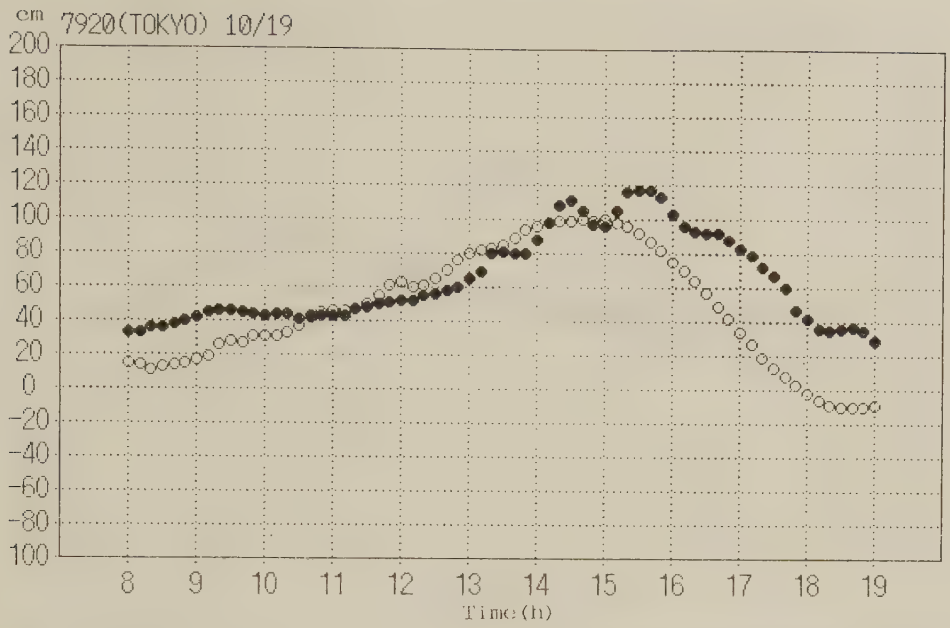

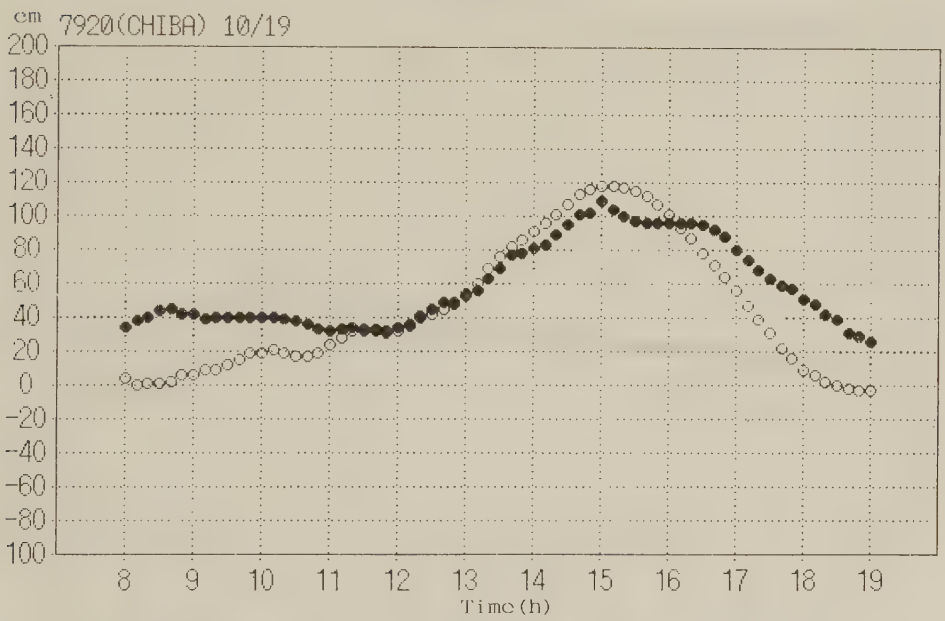

Fig. 5.3.1. Same as Fig. 5.1.1, but the results at Tokyo in case of T7920. (upper)

Fig. 5.3.2. Same as Fig. 5.3.1, but the results at Chiba. (lower)

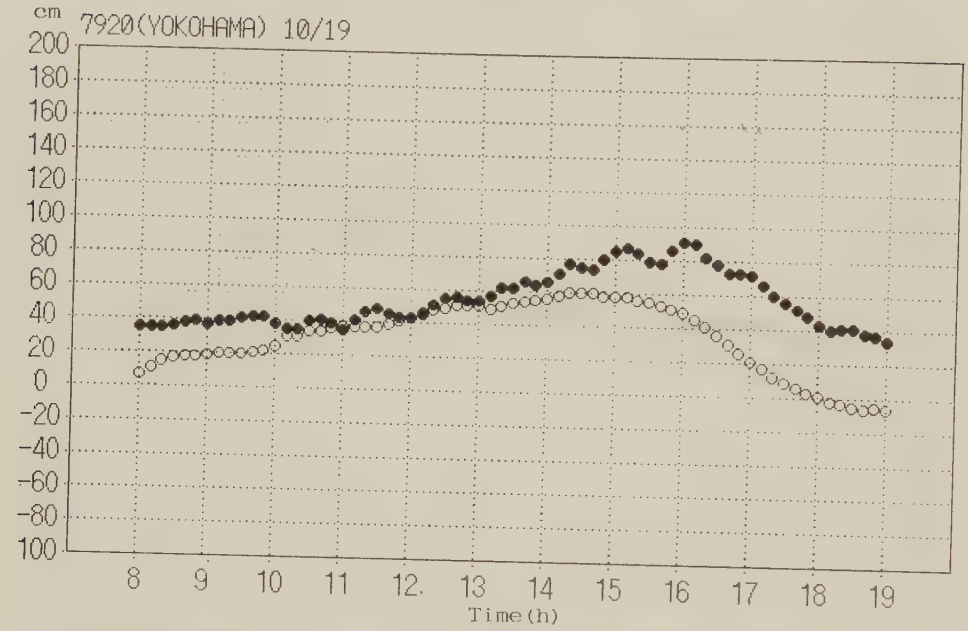

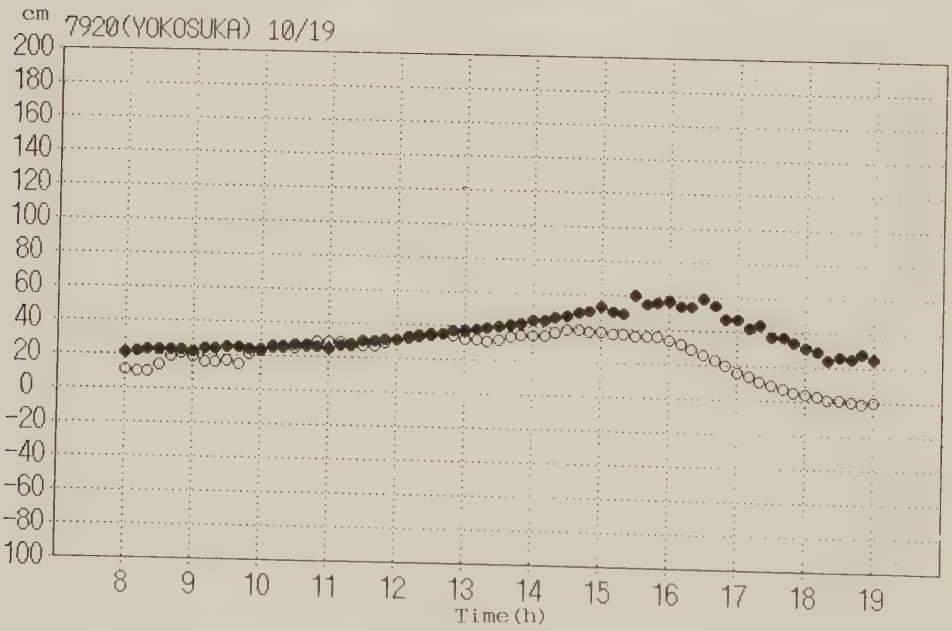

Fig. 5.3.3. Same as Fig. 5.3.1, but the results at Yokohama. (upper)

Fig. 5.3.4. Same as Fig. 5.3.1, but the results at Yokosuka. (lower)

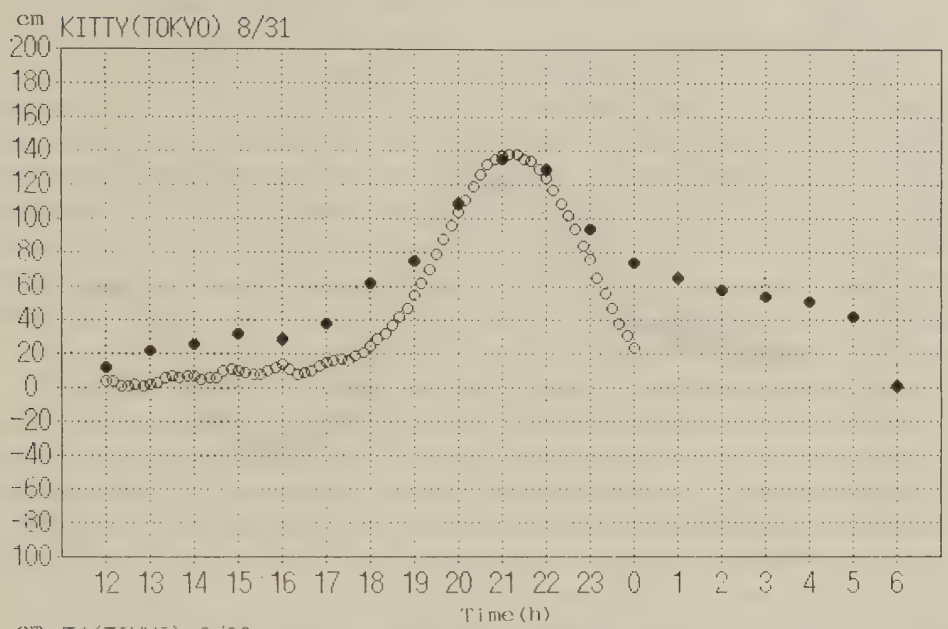

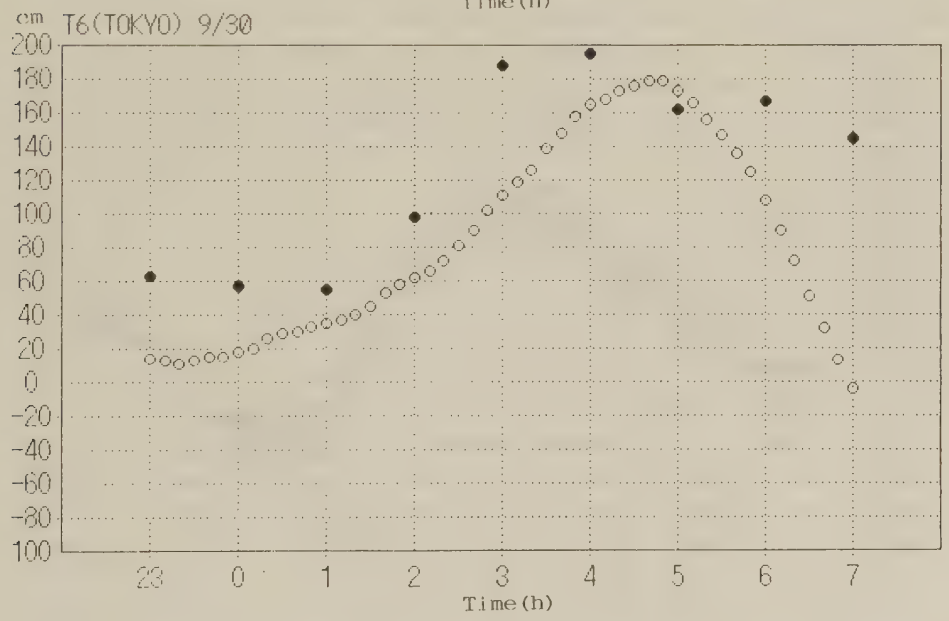

Fig. 5.4. Same as Fig. 5.1.1, but the results at Tokyo in case of the typhoon Kitty. (upper)

Fig. 5.5. Same as Fig. 5.1.1, but the results at Tokyo in case of the typhoon T6. (lower)

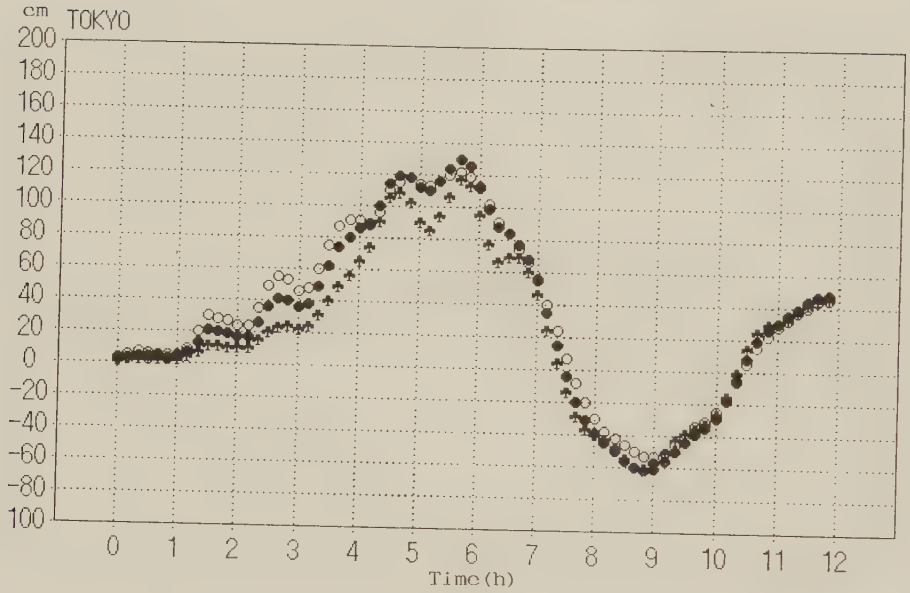

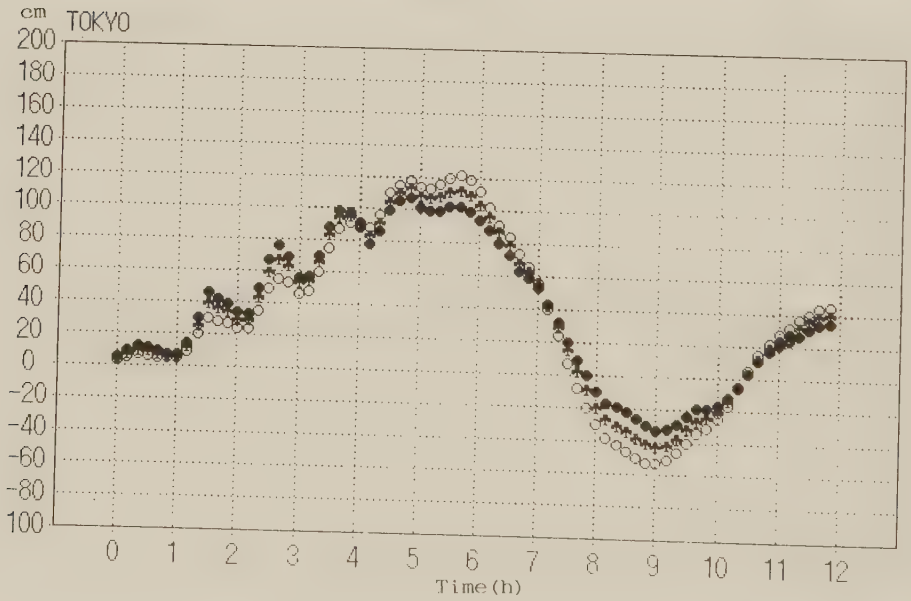

Fig. 6.1. Variation of calculated storm surges due to different r_0 in case of T8506. Clubs: $r_0=20$ km, Solid circles: $r_0=40$ km, Open circles: $r_0=60$ km. (upper)

Fig. 6.2. Same as Fig. 6.1 but Open circles: $r_0=60$ km, Clubs: $r_0=80$ km, Solid circles: $r_0=100$ km. (lower)

7. Accuracy of the numerical prediction of storm surge

In the past, the empirical formula such as

$$H=k_1(1010-P_0)+k_2W^2\cos(\theta-\theta_0)$$

has been used for storm surge prediction of JMA on real time basis, where H is the predicted peak surge, P_0 the predicted minimum pressure, W the predicted maximum wind speed and θ the predicted wind direction. Also, k_1, k_2 and θ_0 are the empirical constants which are determined by the least square method with the past data of storm surges and corresponding meteorological elements at the same place. Table 1 shows the comparison among observed storm surges, predicted storm surges with empirical formula and numerical prediction for above-mentioned five cases. It includes four kinds of empirical prediction. The prediction of a1 and a2 are performed by a formula which was established with old data for Tokyo Bay and b1 and b2 are performed by newly determined formula. Suffix 1 means that observed minimum pressure, wind speed and direction are assigned to P_0, W and θ respectively, on the other hand, in case of suffix 2, the calculated results of meteorological elements by dynamical methods are assigned to P_0 and W, supposing null for θ. Predicted errors are indicated by the percent on the observed peak surge in the parenthesis and the sum of the absolute percent and the means of them are also shown in the lower lines in the table. The result indicates that the prediction with the numerical method is best and the next is a1. The error rate of the numerical method is lower than 10 percent.

The difference between results of a2 and that of b2 is simply discussed below. The coefficients of the formula a2 are determined by the recent observed data and we expect the good agreement between the results with the formula a2 and the observed storm surges, but the table shows that the prediction of a2 is the worst. The reason is considered as follows. The empirical constants of a2 were determined by the data observed at Tokyo District Meteorological Observatory. The winds at the office are rather weaker than at the bay because of the geographical condition. But Fujita's formula does not include the attenuation effect of wind over the land and the wind with the formula is stronger than observed wind over the land. As a result, the formula a2 using the wind of eq. (6) predicts over-estimated storm surges. On the other hand, the formula b2 is based on the older

Table 1 Comparison between the empirical formula and this study (cm)

typhoon	Observed residual	Empirical formula(*)				This study
		a1	b1	a2	b2	
T6	206	244 (+18)	270 (+31)	261 (+27)	228 (+11)	178 (−14)
KITTY	141	75 (−47)	93 (−34)	154 (+ 9)	138 (− 2)	137 (− 3)
7920	116	109 (− 6)	78 (−33)	142 (+22)	120 (+ 3)	99 (−15)
8218	91	93 (+ 2)	74 (−19)	133 (+46)	111 (+22)	96 (+ 5)
8506	127	117 (− 8)	79 (−38)	197 (+55)	174 (+45)	122 (− 4)
Error	Sum	(81)	(155)	(159)	(83)	(41)
	mean	16	31	32	17	8

(*) a1,a2: H=2.332*(1010-P_0)+0.112*W*W*COS($\theta-\theta_0$)
b1,b2: H=1.059*(1010-P_0)+0.138*W*W*COS($\theta-\theta_1$)
See the text about the differences of suffixes.

Acknowledgement

The author is grateful to Dr. S. Arakawa, Director of Oceanographical Division of Marine Department, for critical comments about the draft of this paper.

References

Japan Meteorological Agency (1988): Tide Tables for the Year 1989, Reference data for storm surge forecast, p. 319 (in Japanese).

Konishi, T., T. Kinosita, and T. Takahashi (1985): Studies on storm surges in Tidal Estuaries, Seventh Joint Meeting U.S.-Japan Panel on Wind and Seismic Effects UJNR, 735–750.

Konishi, T., E. Kamihira and T. Segawa (1986): Storm surges of the typhoon 8506 and induced secondary undulations, Tenki Vol. 33 (6), 13–20 (in Japanese).

Miyazaki, M., T. Ueno and S. Unoki (1961, 1962): The theoretical investigations of typhoon surges along the Japanese coast (I), Oceanogr. Mag., **13** (1), 51–75; (II), Oceanogr. Mag., **13** (2), 103–117.

Tokyo Metropolitan Government (1986): Disaster prevention for Tokyo Bay, pp. 79 (in Japanese).

Unoki, S., I. Isozaki and S. Otsuka (1964): Simulations of storm surges in Tokyo Bay, Report of the Second District Port Construction Bureau pp. 125 (in Japanese).

実時間での高潮の力学的な数値予測モデルについて

小 西 達 男

(気象庁海洋気象部)

実時間で使用する高潮の力学的な数値予測モデルの一手法を提案する．基本的には，従来の高潮の再現計算と同様な方法を用いている．特に，気圧分布について，藤田の式を，台風域内の風速分布については，宮崎が行った定式化を用いたが，実時間での使用を考慮して，モデルに含まれるパラメータをできるだけ固定した．その結果，実時間でそれぞれの台風について定めるべきパラメータは，台風の初期位置（経度，緯度），台風の移動速度と進路，最低気圧及び最大風速半径の 6 個となった．

東京湾に過去に大きな高潮を起こした 5 つの台風について，それぞれ観測された気象要素から 6 個のパラメータを定め，検証計算を行った．その結果，観測値に適合するパラメータを選択することにより，東京について 10% の誤差で最大偏差を予測できることがわかった．これは，従来使用してきた実験式よりも良い精度となっている，また，湾内の各地点についてもほぼ同様な程度の精度をもつが，外洋に面した地点については，誤差が大きい．なお，現在のモデルが 12 時間の予測に要する CPU タイム（気象庁数値予報用の計算機による）は 90 秒となっており，実時間での計算処理が可能である．

数値計算法のなかで，開放境界に関して従来のものとは異なる境界条件を提案した．この境界条件は，従来高潮計算で使用されてきた境界での大気圧に水位がバランスする条件，及び津波計算等で使用されてきた放射条件を折衷したものであるが，前者の境界条件を使うときに計算上あらわれる振動を減少させ，後者を用いた場合に生じる水位の低下を防ぐという利点をもつ．

The Oceanographical Magazine
Vol. 39, Nos. 1-2, pp. 43 to 58, March 1989

Statistical study on sea ice in the Okhotsk Sea observed by GMS for 10 years

Yuji KANO, Kiyotomi SATO and Shoumei SHIRATO
Japan Meteorological Agency

(Received August 26, 1988; Accepted November 28, 1988)

Abstract: Many kinds of statistical characteristics on sea ice in the Okhotsk Sea were derived from sea ice charts for 10 years since the 1977/78 winter, when images from the Geostationary Meteorological Satellite (GMS) had been first applied to sea ice condition analysis.

Sea ice charts every 5 days were digitized at the geographical grid points by means of a personal computer with a digitizing equipment. Grid point values on sea ice concentration, which were read every 0.25 degree along longitude and every 0.5 degree along latitude by the personal computer, were stored into floppy disks as basic data files.

Probability of sea ice existence and mean concentration when sea ice exists were calculated at each grid point every 5 days from the basic digital data files. Sea ice distribution charts for mean, maximum and minimum extent, probability charts of sea ice existence and charts on mean concentration when sea ice exists were drawn every 5 days from the statistical values. For instance, when a sea ice chart is compared with the probability chart of sea ice existence on the same date, the ice extent can be estimated with quantitative expression like "normal": 30–70%, "wide" ("narrow"): 10–30% (70–90%) or "very wide" ("very narrow"): 0–10% (90–100%).

Sea ice extent was also calculated for 6 regions of the Okhotsk Sea and the adjacent seas every 5 days during 10 years, and year to year and annual variations of sea ice extent were figured. Six regions consists of the north, the middle and the south of the Okhotsk Sea, the Japan Sea, the western region of Soya Strait and the Pacific. Annual variations of mean, maximum and minimum sea ice extent were also shown for every regions.

Year to year and annual variations of sea ice extent will contribute to study the interaction between sea ice and climate.

1. Introduction

In every winter season sea ice is formed and extends in the Okhotsk Sea, where it affects largely fishing boats and merchant vessels in navigation. Sea ice survey has been so difficult due to the serious environment of nature for observation that the amount of sea ice data in the high seas has been quite small. The verious kinds of earth observation satellites enabled the comprehensive survey of sea ice conditions in the Okhotsk Sea. Sea ice analysis in the whole area of the Okhotsk Sea began in 1967 based on the imagery data of ESSA, which was succeeded by NOAA Satellites. The Geostationary Meteorological Satellite (GMS) was launched in 1977 and since then GMS data have been applied to operational sea ice information service of Japan Meteorological Agency (JMA), whose sea ice charts by the GMS have been accumulated for 10 years with nearly the same qualities (JMA: 1983–).

Acknowledgement

The author is grateful to Dr. S. Arakawa, Director of Oceanographical Division of Marine Department, for critical comments about the draft of this paper.

References

Japan Meteorological Agency (1988): Tide Tables for the Year 1989, Reference data for storm surge forecast, p. 319 (in Japanese).

Konishi, T., T. Kinosita, and T. Takahashi (1985): Studies on storm surges in Tidal Estuaries, Seventh Joint Meeting U.S.-Japan Panel on Wind and Seismic Effects UJNR, 735–750.

Konishi, T., E. Kamihira and T. Segawa (1986): Storm surges of the typhoon 8506 and induced secondary undulations, Tenki Vol. 33 (6), 13–20 (in Japanese).

Miyazaki, M., T. Ueno and S. Unoki (1961, 1962): The theoretical investigations of typhoon surges along the Japanese coast (I), Oceanogr. Mag., **13** (1), 51–75; (II), Oceanogr. Mag., **13** (2), 103–117.

Tokyo Metropolitan Government (1986): Disaster prevention for Tokyo Bay, pp. 79 (in Japanese).

Unoki, S., I. Isozaki and S. Otsuka (1964): Simulations of storm surges in Tokyo Bay, Report of the Second District Port Construction Bureau pp. 125 (in Japanese).

実時間での高潮の力学的な数値予測モデルについて

小　西　達　男

（気象庁海洋気象部）

実時間で使用する高潮の力学的な数値予測モデルの一手法を提案する．基本的には，従来の高潮の再現計算と同様な方法を用いている．特に，気圧分布について，藤田の式を，台風域内の風速分布については，宮崎が行った定式化を用いたが，実時間での使用を考慮して，モデルに含まれるパラメータをできるだけ固定した．その結果，実時間でそれぞれの台風について定めるべきパラメータは，台風の初期位置（経度，緯度），台風の移動速度と進路，最低気圧及び最大風速半径の 6 個となった．

東京湾に過去に大きな高潮を起こした 5 つの台風について，それぞれ観測された気象要素から 6 個のパラメータを定め，検証計算を行った．その結果，観測値に適合するパラメータを選択することにより，東京について 10% の誤差で最大偏差を予測できることがわかった．これは，従来使用してきた実験式よりも良い精度となっている，また，湾内の各地点についてもほぼ同様な程度の精度をもつが，外洋に面した地点については，誤差が大きい．なお，現在のモデルが 12 時間の予測に要する CPU タイム（気象庁数値予報用の計算機による）は 90 秒となっており，実時間での計算処理が可能である．

数値計算法のなかで，開放境界に関して従来のものとは異なる境界条件を提案した．この境界条件は，従来高潮計算で使用されてきた境界での大気圧に水位がバランスする条件，及び津波計算等で使用されてきた放射条件を折衷したものであるが，前者の境界条件を使うときに計算上あらわれる振動を減少させ，後者を用いた場合に生じる水位の低下を防ぐという利点をもつ．

The Oceanographical Magazine
Vol. 39, Nos. 1-2, pp. 43 to 58, March 1989

Statistical study on sea ice in the Okhotsk Sea observed by GMS for 10 years

Yuji KANO, Kiyotomi SATO and Shoumei SHIRATO
Japan Meteorological Agency

(Received August 26, 1988; Accepted November 28, 1988)

Abstract: Many kinds of statistical characteristics on sea ice in the Okhotsk Sea were derived from sea ice charts for 10 years since the 1977/78 winter, when images from the Geostationary Meteorological Satellite (GMS) had been first applied to sea ice condition analysis.

Sea ice charts every 5 days were digitized at the geographical grid points by means of a personal computer with a digitizing equipment. Grid point values on sea ice concentration, which were read every 0.25 degree along longitude and every 0.5 degree along latitude by the personal computer, were stored into floppy disks as basic data files.

Probability of sea ice existence and mean concentration when sea ice exists were calculated at each grid point every 5 days from the basic digital data files. Sea ice distribution charts for mean, maximum and minimum extent, probability charts of sea ice existence and charts on mean concentration when sea ice exists were drawn every 5 days from the statistical values. For instance, when a sea ice chart is compared with the probability chart of sea ice existence on the same date, the ice extent can be estimated with quantitative expression like "normal": 30–70%, "wide" ("narrow"): 10–30% (70–90%) or "very wide" ("very narrow"): 0–10% (90–100%).

Sea ice extent was also calculated for 6 regions of the Okhotsk Sea and the adjacent seas every 5 days during 10 years, and year to year and annual variations of sea ice extent were figured. Six regions consists of the north, the middle and the south of the Okhotsk Sea, the Japan Sea, the western region of Soya Strait and the Pacific. Annual variations of mean, maximum and minimum sea ice extent were also shown for every regions.

Year to year and annual variations of sea ice extent will contribute to study the interaction between sea ice and climate.

1. Introduction

In every winter season sea ice is formed and extends in the Okhotsk Sea, where it affects largely fishing boats and merchant vessels in navigation. Sea ice survey has been so difficult due to the serious environment of nature for observation that the amount of sea ice data in the high seas has been quite small. The verious kinds of earth observation satellites enabled the comprehensive survey of sea ice conditions in the Okhotsk Sea. Sea ice analysis in the whole area of the Okhotsk Sea began in 1967 based on the imagery data of ESSA, which was succeeded by NOAA Satellites. The Geostationary Meteorological Satellite (GMS) was launched in 1977 and since then GMS data have been applied to operational sea ice information service of Japan Meteorological Agency (JMA), whose sea ice charts by the GMS have been accumulated for 10 years with nearly the same qualities (JMA: 1983–).

These 10 years data were digitized at geographycal grid points for our statistical calculation. The probability of sea ice existence and the mean concentration when sea ice exists are calculated at all grid points every 5 days in addition to sea ice extent. Anomaly of sea ice condition can be easily known in terms of using these results. For example, the comparison of a given sea ice chart with the probability chart provides a quantitative expression that the ice extent in the chart is "normal": 30–70%, "wide" ("narrow"): 10–30% (70–90%) or "very wide" ("very narrow"): 0–10% (90–100%). Moreover, if sea ice existence is expected in the navigation route, the statistically predicted concentration in the area can be derived from the chart of mean concentration.

The statistical charts involving only mean, maximum and minimum ice extents from 1971 to 1980 have already been published (JMA: 1982). The 30 years summary report published in 1988 includes synthetic information on sea ice (JMA: 1988). Some other papers reported on the relation between sea ice and climate based on sea ice statistics. The present paper provides quantitative and comprehensive information about the statistical characteristics based on the digital sea ice data.

These digital sea ice data in the Okhotsk Sea are also able to contribute the establishment of global sea ice data bank which the World Meteorological Organization (WMO) is now progressing for World Climate Research Program (WCRP). Though SIGRID format, which can represent many kinds of sea ice parameters at geographical grid points, was adopted for global sea ice data bank, digital data in the present study will be easily transformed into this international format. Moreover the digitizing method of sea ice charts is applicable to obtaining the initial data set for numerical forecasting model of sea ice now being developed.

2. Data processing

Sea ice condition charts involving ice edges and concentrations have been issued for operational marine meteorological service through radio facsimile, JMH, on Tuesday and Friday from December to May based mainly on the GMS data. Besides, sea ice charts by more precise analysis have been compiled every 5 days for statistical purpose in an annual summary. The present paper referred to the latter original charts for numerical statistics. For digitizing sea ice charts, each area of 1 by 1 degree square is divided by 0.25 degree along longitude and 0.5 degree along latitude into 8 areas with a grid point at the center. Concentration data of sea ice identified at all grid points were stored into floppy disks as basic data files.

Outline of the method of digitizing sea ice charts is following;

(1) Lines which classify concentrations in the chart are traced on a digitizing equipment (GRAPHTEC Digitizer KD-4600) and are reproduced on a display of a personal computer (NEC PC-9801 VM) together with the geographical map.

(2) Every sea ice regions and land area are painted with a color according to the rank of classified concentration and land. A sample of sea ice charts is shown in Fig. 1.

(3) The concentration of sea ice on each grid point is derived by reading the color of

Fig. 1. A sample chart input by the digitizing equipment (31 January 1987). Tile marks denote the sea ice concentration of the area based on the international system of sea ice symbols. ▦: 9–10, ▤: 7–8, ▥: 4–6, and ⁘: 1–3. In order to digitize the chart, each area is painted with a color according to the concentration instead of tile mark on the display of a personal computer and the dot color is read out at the grid points.

the dot at the corresponding grid point on the display.

3. Methods and results of statistical calculation

Three kinds of sea ice charts are prepared by statistics of grid point values for 10 years. All charts are drawn every 5 days from December to May but shown only on the 15th and the end of the month in the present paper.

(1) Sea ice edges for mean, maximum and minimum extent

Sea ice edge for maximum extent is between grid points where sea ice exists at least once and where sea ice never exists among 10 times for 10 years. Minimum ice edge is between grid points where sea ice exists 10 and 9 times. Sea ice edge for mean extent is on the position where sea ice exists 5 times for 10 years. A sample chart drawn by the computer with numerics denoting probability is shown in Fig. 2. The charts of sea ice edge for

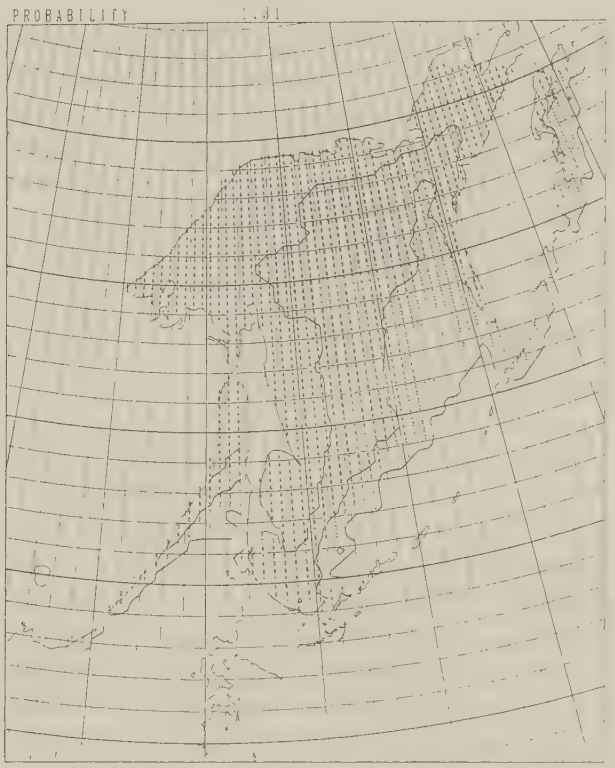

Fig. 2. A sample chart of sea ice edges for mean, maximum and minimum extent together with numerics denoting probability in tenth drawn by the computer (31 January).

mean, maximum and minimum extent are shown in Fig. 3.

(2) Probability of sea ice existence

Probability of sea ice existence is divided into 5 ranks such as 0–10%, 10–30%, 30–70%, 70–90% and 90–100%. These ranks are corresponding to statistical terms of "very wide", "wide", "normal", "narrow" and "very narrow". Probability charts of sea ice existence are shown in Fig. 4.

(3) Mean concentration when sea ice exists

Mean concentration is obtained by averaging concentrations only when sea ice exists. Tile marks on the charts indicate concentration according to the international system of sea ice symbols. Mean sea ice concentration charts are shown in Fig. 5.

(4) Year to year and annual variation of sea ice extent

The Okhotsk Sea and the adjacent seas are divided into 6 regions to study the variation of sea ice extent in each regions. Six regions are the south, the middle and the north of the Okhotsk Sea, the Japan Sea, the western region of Soya Strait and the Pacific as shown in Fig. 6. Year to year and annual variations of sea ice extent are shown in Fig. 7 with the

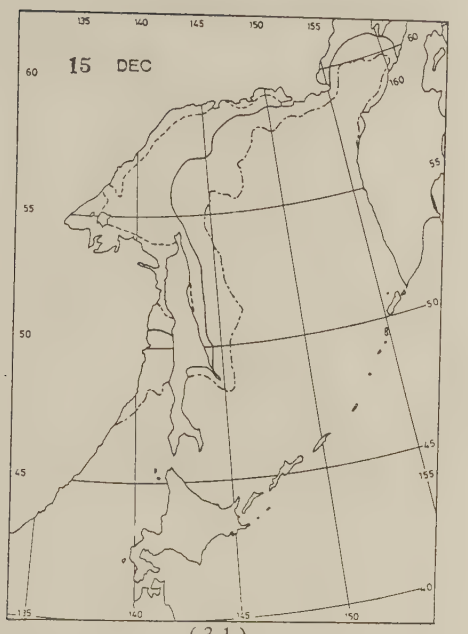

(3-1)

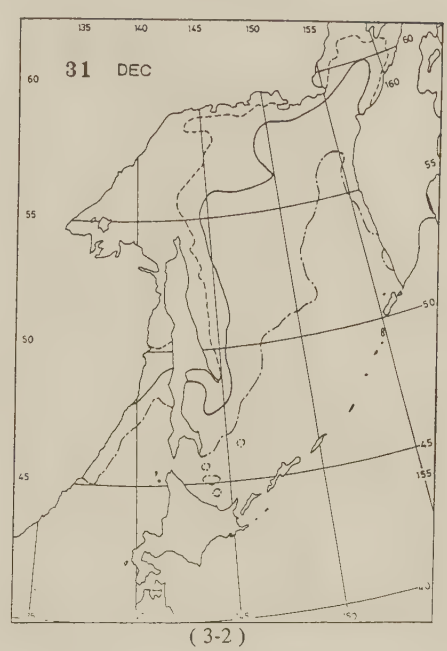

(3-2)

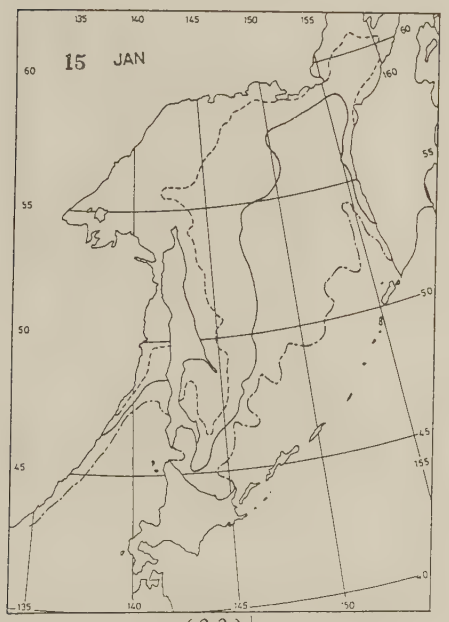

(3-3)

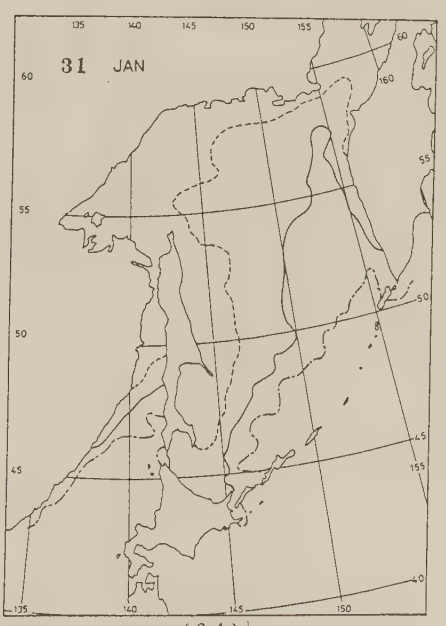

(3-4)

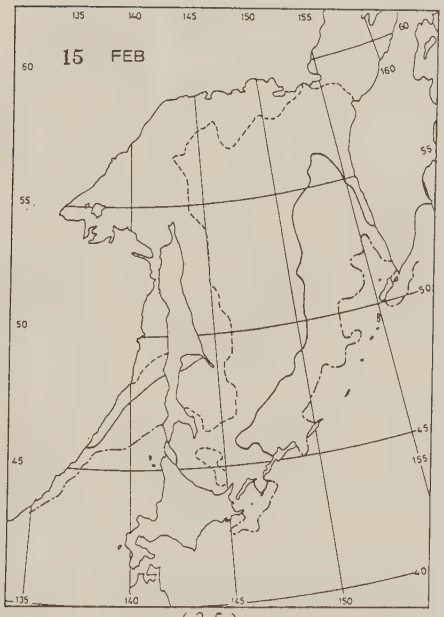
15 FEB
135
140
145
150
155
60
55
50
45
40
160

(3-5)

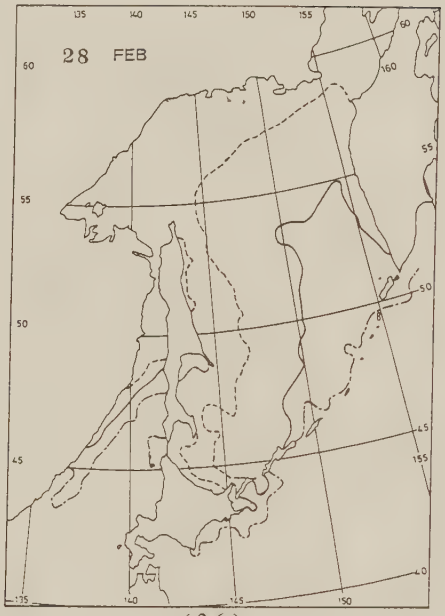
28 FEB
135
140
145
150
155
60
55
50
45
40
160

(3-6)

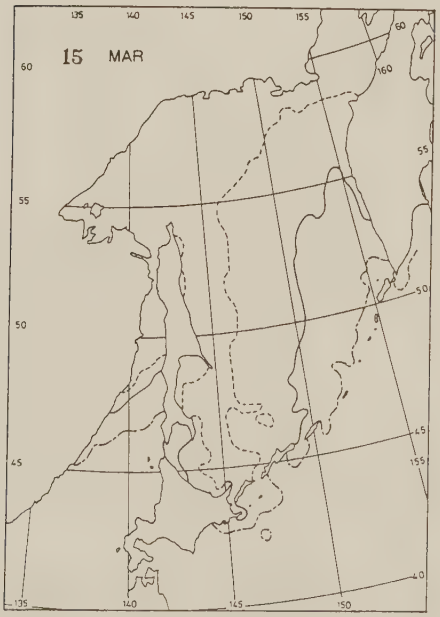
15 MAR
135
140
145
150
155
60
55
50
45
40
160

(3-7)

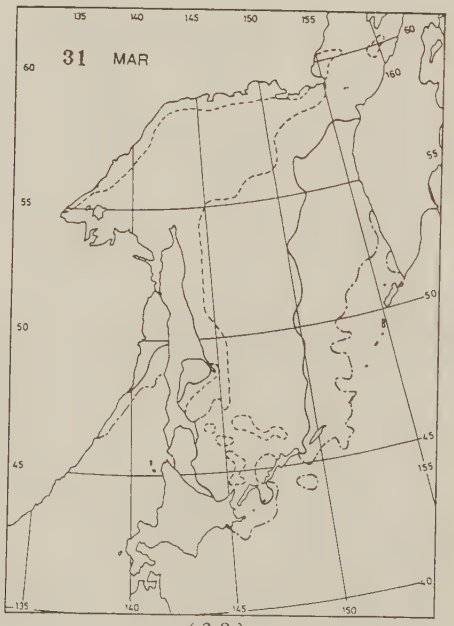
31 MAR
135
140
145
150
155
60
55
50
45
40
160

(3-8)

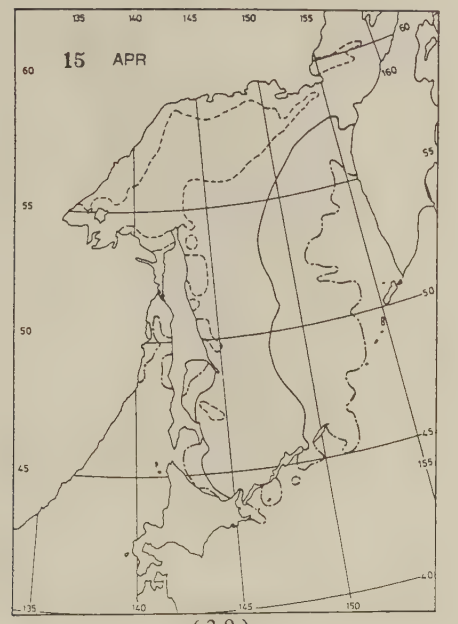

(3-9)

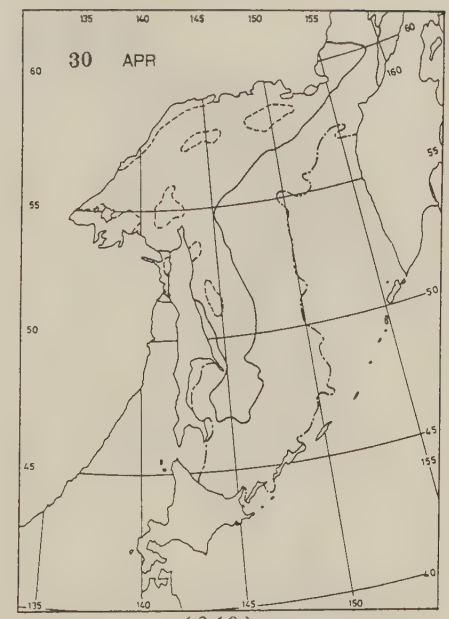

(3-10)

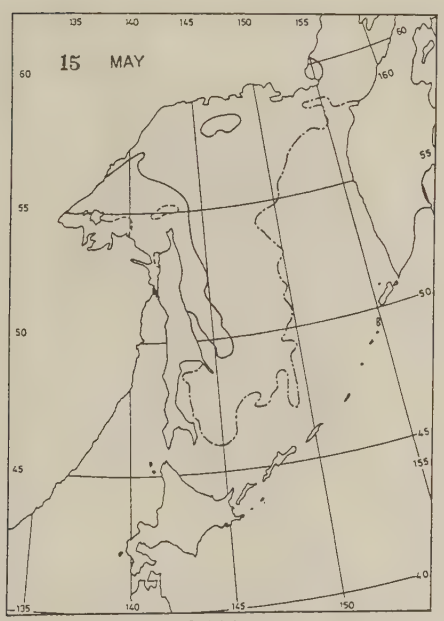

(3-11)

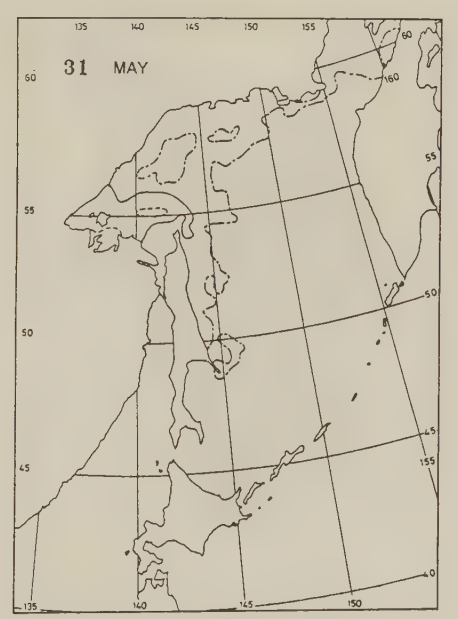

(3-12)

Fig. 3. Charts of sea ice edges for mean, minimum and maximum extent on the 15th and the end of the month from December to May. Mean: ——, minimum: ---- and maximum: -·-·-.

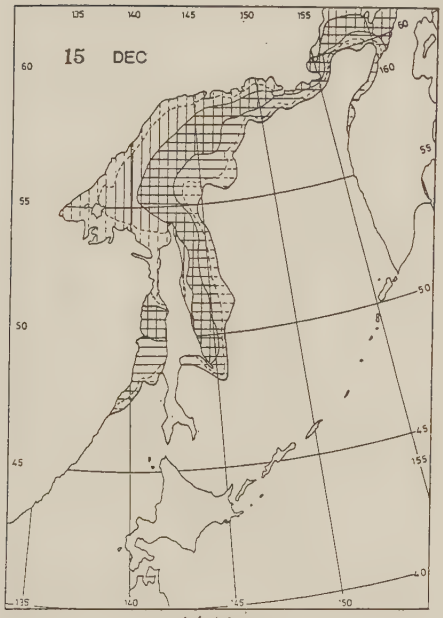

(4-1)

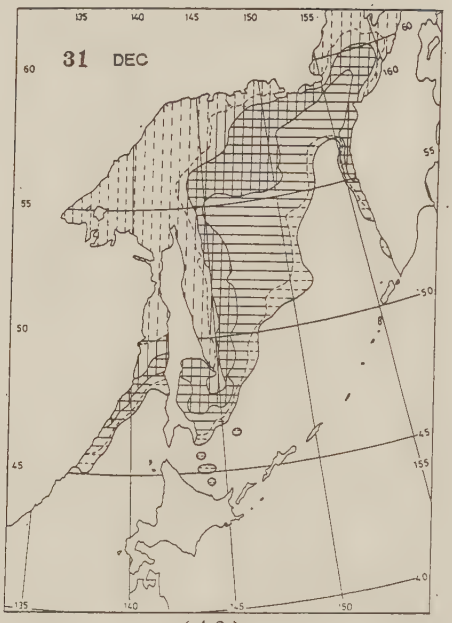

(4-2)

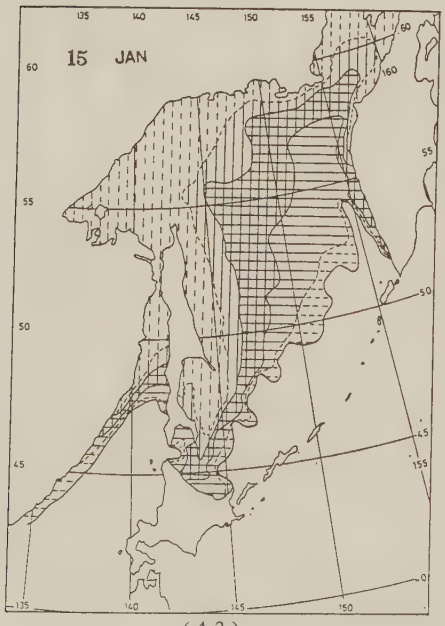

(4-3)

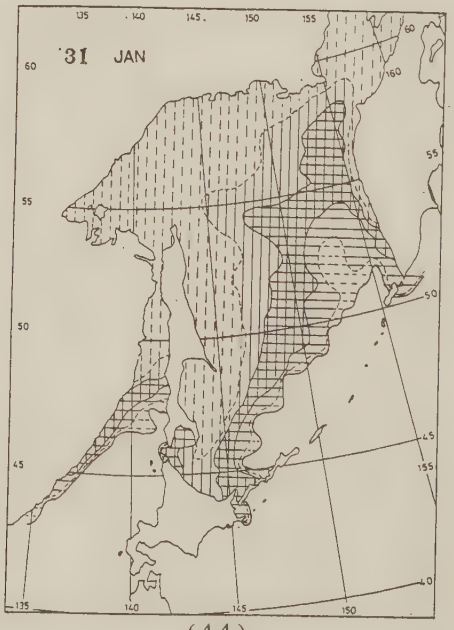

(4-4)

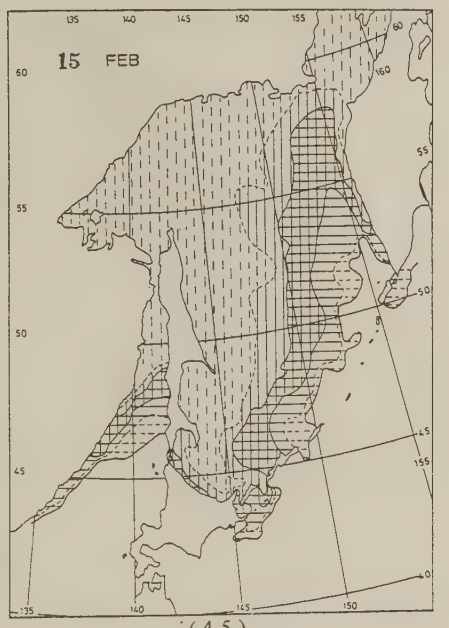

(4-5)

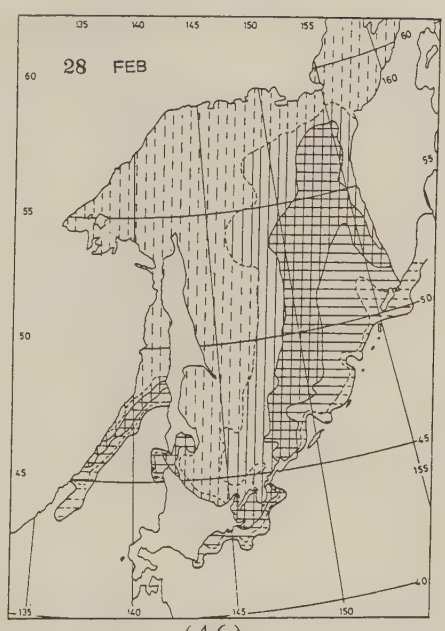

(4-6)

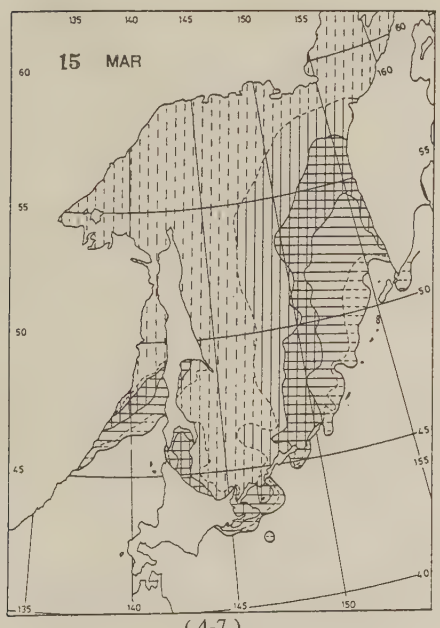

(4-7)

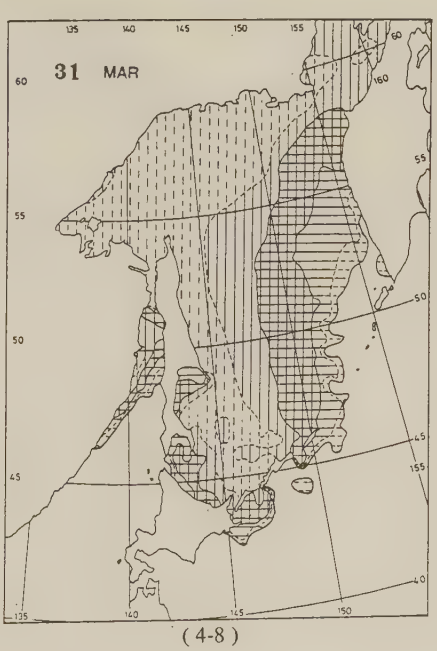

(4-8)

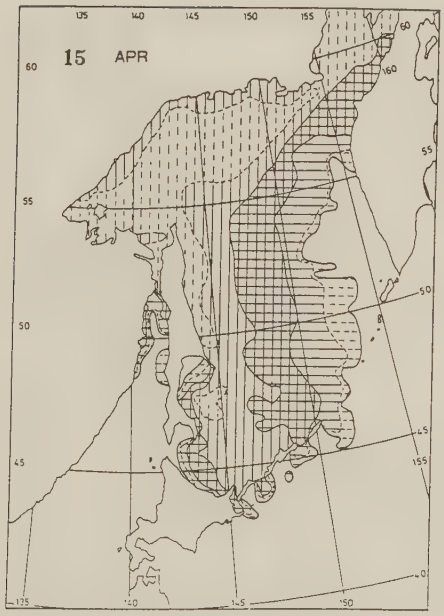

(4-9)

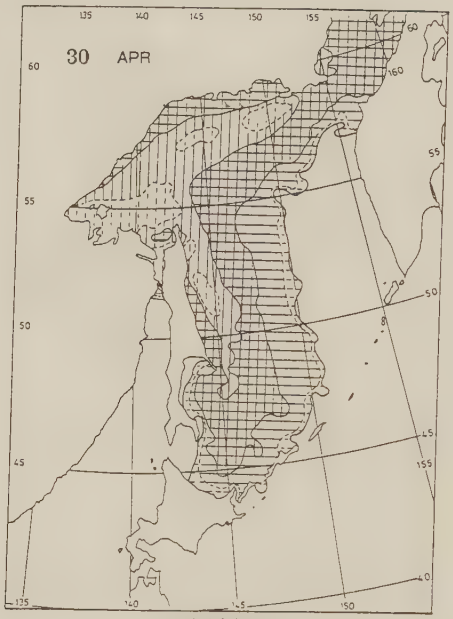

(4-10)

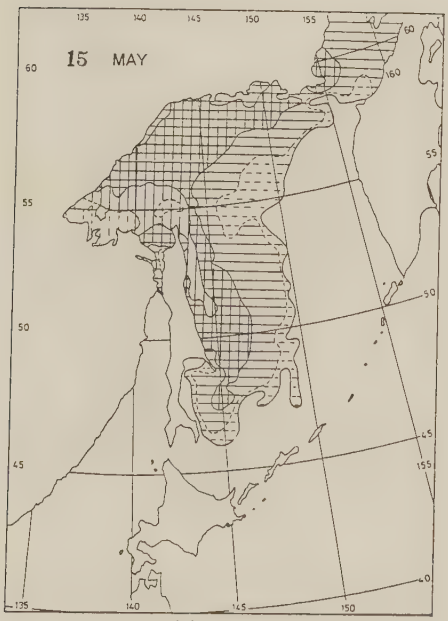

(4-11)

(4-12)

Fig. 4. Probability charts of sea ice existence on the 15th and the end of the month from December to May. ▤: 0–10%, ▤: 10–30%, ▤: 30–70%, ▤: 70–90%, and ▤: >90%.

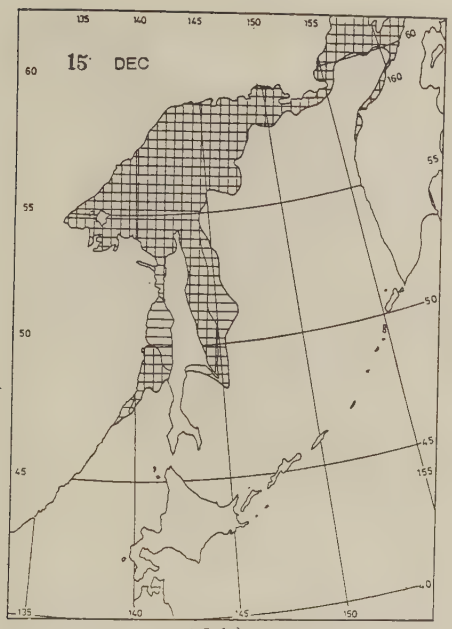
15 DEC
135
140
145
150
155
60
55
50
45
40

(5-1)

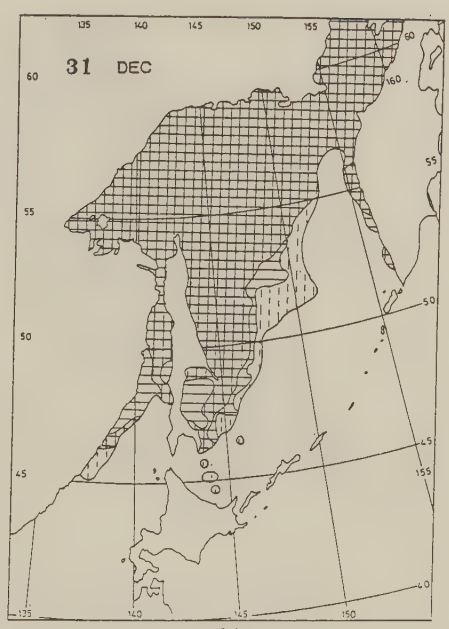
31 DEC
135
140
145
150
155
60
55
50
45
40

(5-2)

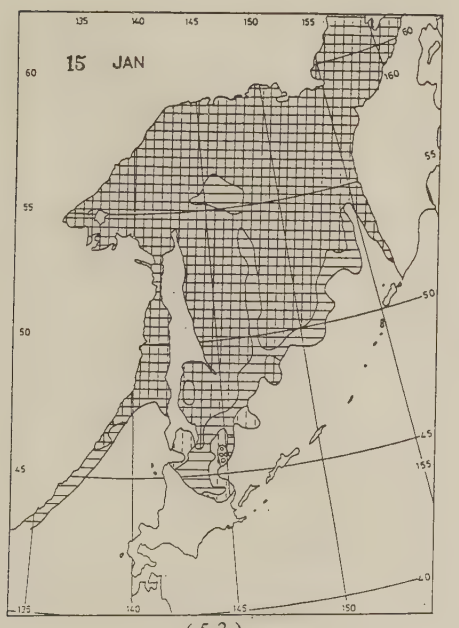
15 JAN
135
140
145
150
155
60
55
50
45
40

(5-3)

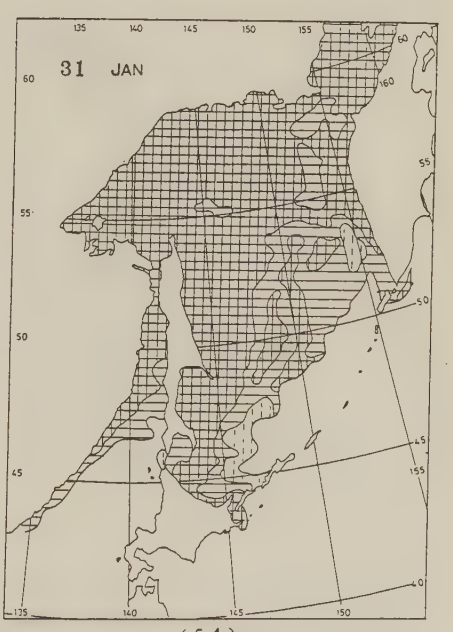
31 JAN
135
140
145
150
155
60
55
50
45
40

(5-4)

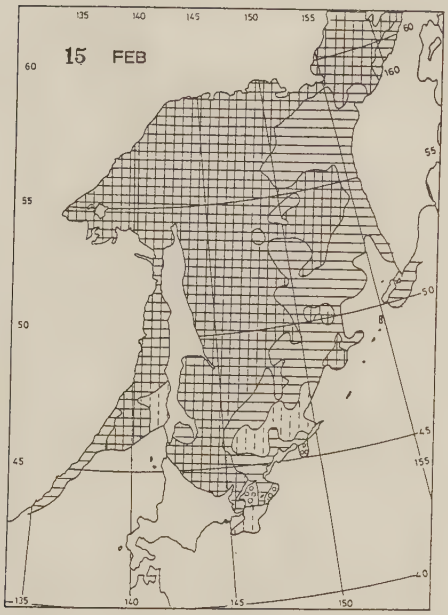
15 FEB
135
140
145
150
155
60
55
50
45
40

(5-5)

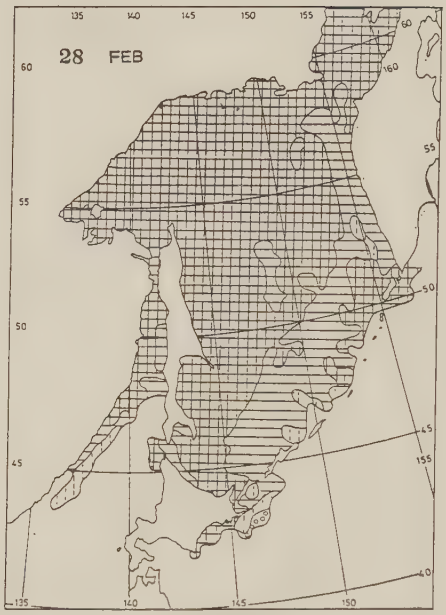
28 FEB
135
140
145
150
155
60
55
50
45
40

(5-6)

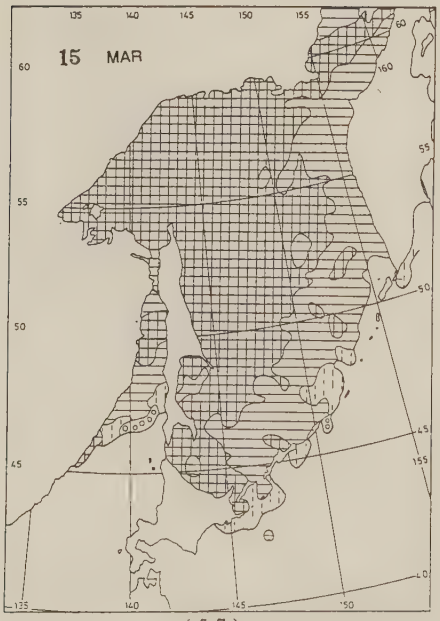
15 MAR
135
140
145
150
155
60
55
50
45
40

(5-7)

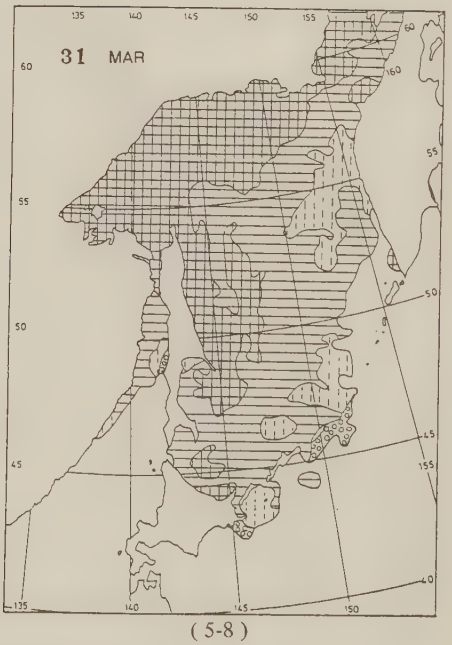
31 MAR
135
140
145
150
155
60
55
50
45
40

(5-8)

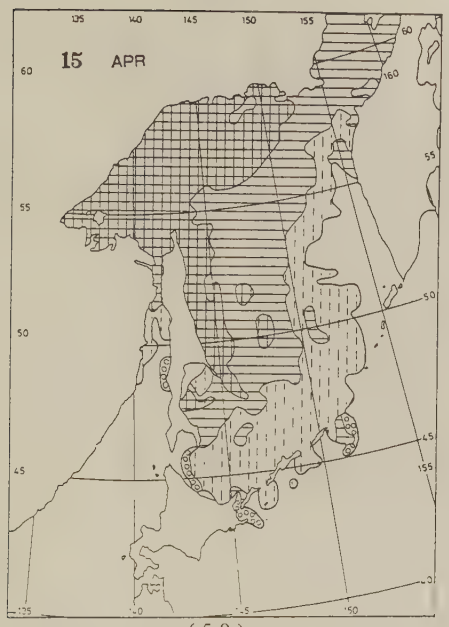

(5-9)

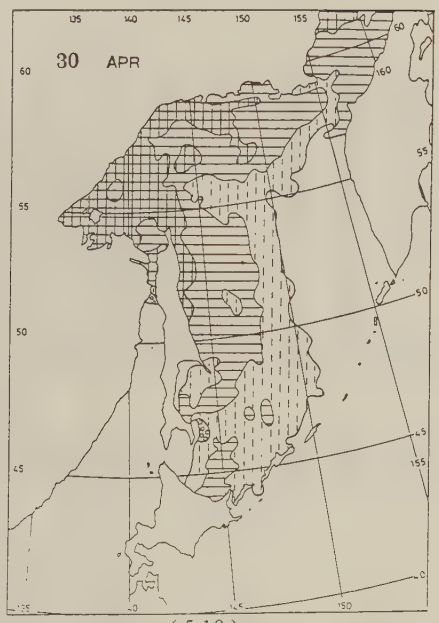

(5-10)

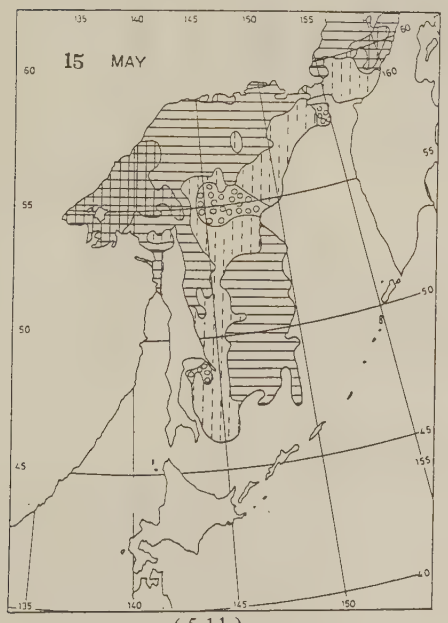

(5-11)

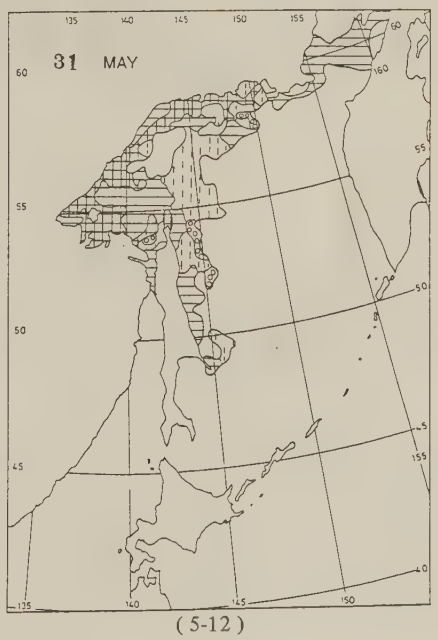

(5-12)

Fig. 5. Charts of mean sea ice concentration when sea ice exists on the 15th and the end of the month from December to May. ▦: 9–10, ▤: 7–8, ▥: 4–6, and ▥: 1–3.

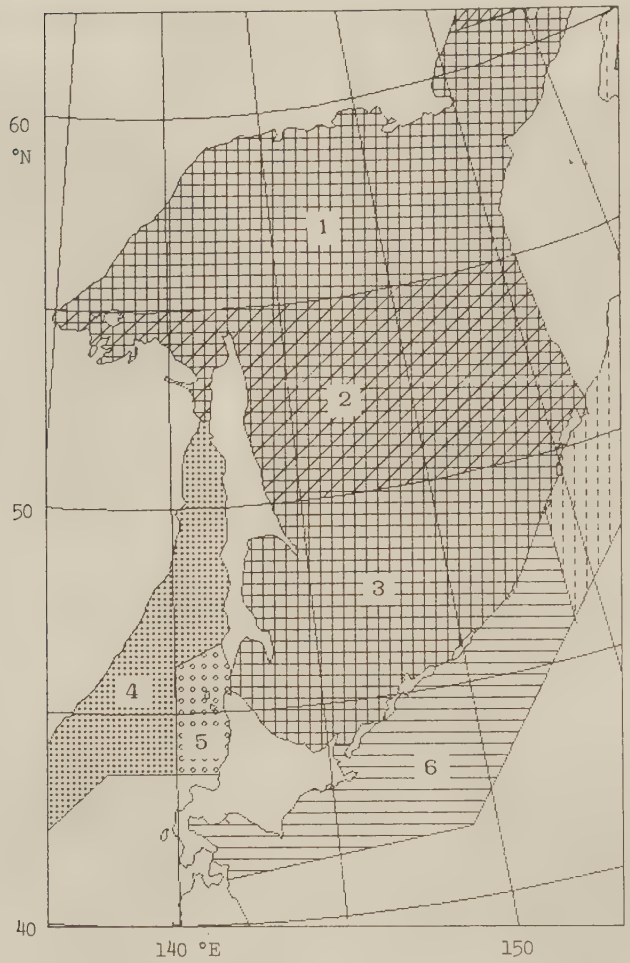

Fig. 6. Six regions in the Okhotsk Sea and the adjacent seas. (1) the north, (2) the middle, (3) the south of the Okhotsk Sea, (4) the Japan Sea, (5) the western region of Soya Strait and (6) the Pacific.

annual variation of mean, maximum and minimum extent for 10 years.

Attention to be paid in Fig. 7 is that in February 1985 sea ice extent in the region west of Soya Strait does not indicate the sea ice flow from the Okhotsk Sea through the strait. Because in these days the entire region was frozen up west of Soya Strait and the sea ice through it merged into the one in the Japan Sea.

References

AKAGAWA, M. (1984): Sea ice and climate. Weather Service Bulletin, **51**, 411–437 (in Japanese).

ASO, T. (1986): Sea ice distribution in the Sea of Okhotsk and meteorological condition, in "Improvement of short and long term forecasting method on sea ice", Tech. Rep. Special

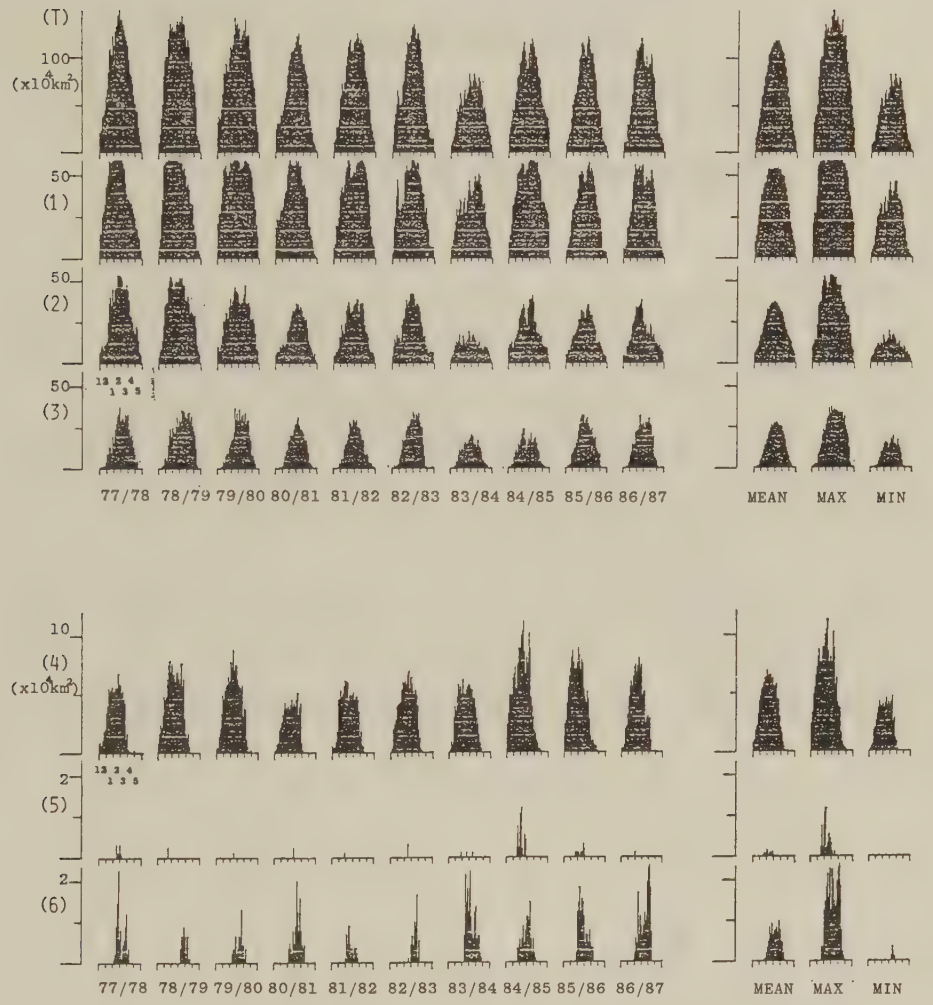

Fig. 7. Year to year and annual variations of sea ice extent in (T) whole area of the Okhotsk Sea, (1) the north (50–61°N), (2) the middle (45–50°N) and (3) the south (<45°N) of the Okhotsk Sea, (4) the Japan Sea (>135°E), (5) the western region of Soya Strait and (6) the Pacific. Annual variations of mean, maximum and minimum sea ice extent for 10 years are also shown.

Edition published by Sapporo district observatory and Hakodate marine observatory, No. 35, 5–14 (in Japanese).

Japan Meteorological Agency (1982): Statistical data on sea ice (in Japanese).

Japan Meteorological Agency (1983–): The results of sea ice observation, No. 1–, in Japanese with English figure captions.

Japan Meteorological Agency (1988): Report on 30 years of observation of sea ice, Tech. Rep. JMA, No. 109, in Japanese with English outline.

SHINOHARA, Y. and N. SHIKAMA (1988): Marine climatological atlas of the Sea of Okhotsk, Tech. Rep. Meteorol. Inst. No. 23, in Japanese with English outline and figure captions.

The Oceanographical Magazine, Vol. 39, Nos. 1–2 (1989)

オホーツク海の海氷の分布

——気象衛星「ひまわり」による海氷観測結果 10 年の統計——

加納裕二　佐藤清富　白土正明
（気象庁海洋気象部）

要旨

静止気象衛星「ひまわり」の画像を用いて海氷の解析を始めた 1977/78 年冬期から，10 年間のオホーツク海の海氷資料を用いて，統計資料を作成した．気象庁海洋気象部海上気象課に保存されている半旬毎の海氷図を，パソコンとデジタイザを用いてデジタル化する．南北 0.25°，東西 0.5。毎のグリッド点における海氷の密接度をパソコンで読み取り，基本データファイルとした．

基本データファイルから，半旬毎の各グリッド点の海氷の存在確率と，海氷が存在した時の平均密接度を計算した．この統計値を用いて，半旬毎の海氷の平均・最大・最小図，存在確率分布図および海氷が存在する時の平均密接度の図を作成した．ある時の海氷図を海氷の確率分布図と比較することにより，海氷域が平年並：30—70%，やや広い（狭い）：10—30%（70—90%），かなり広い（狭い）：0—10%（90—100%）等の表現が可能となる．

またオホーツク海と周辺海域を 6 つの海域に区分し，オホーツク海全域と各区分海域の海氷面積を半旬毎に計算し，海氷面積の経年変化図を作成した．6 つの海域はオホーツク海北部，中部，南部，日本海，宗谷海峡西側および太平洋である．また各区分海域の平均・最大・最小の海氷面積の季節変動の図も作成した．

海氷面積の経年変化図は，オホーツク海の海氷面積と気候との関係をさぐる基礎資料となろう．

SCIENCE & ENGINEERING LIBRARY

（この刊行物は気象庁の許可を得て複製したものである。）

平成 元年 3月 31日発行

編集者　気　象　庁
東京都千代田区大手町１丁目３番４号

発行所　財団法人　日本気象協会

発行人　町　田　直
東京都千代田区麹町４丁目５番地

印刷所　昌美印刷株式会社
東京都千代田区飯田橋 2-6-1

¥1600